Massively parallel fitness profiling reveals multiple novel enzymes in *Pseudomonas putida* lysine metabolism

Mitchell G. Thompson[1,2,3], Jacquelyn M. Blake-Hedges[1,2,4], Pablo Cruz-Morales[1,2,5], Jesus F. Barajas[2,6], Samuel C. Curran[1,2,7], Christopher B. Eiben[1,2,8], Nicholas C. Harris[3], Veronica T. Benites[1,2], Jennifer W. Gin[1,2], William A. Sharpless[1,2,3], Frederick F. Twigg[8], Will Skyrud[4], Rohith N. Krishna[1,2,4], Jose Henrique Pereira[1,9], Edward E. K. Baidoo[1,2], Christopher J. Petzold[1,2], Paul D. Adams[1,9,10], Adam P. Arkin[10,11], Adam M. Deutschbauer[3,11], Jay D. Keasling[1,2,8,10,12]

[1]Joint BioEnergy Institute, 5885 Hollis Street, Emeryville, CA 94608, USA.

[2]Biological Systems & Engineering Division, Lawrence Berkeley National Laboratory, Berkeley, CA 94720, USA.

[3]Department of Plant and Microbial Biology, University of California, Berkeley, CA 94720, USA

[4]Department of Chemistry, University of California, Berkeley, CA 94720, USA

[5]Centro de Biotecnología FEMSA, Tecnológico de Monterrey, NL, Mexico

[6]Department of Energy Agile BioFoundry, Emeryville, CA 94608, USA

[7]Comparative Biochemistry Graduate Group, University of California, Berkeley, CA 94720, USA

[8]Department of Chemical and Biomolecular Engineering, University of California, Berkeley, CA 94720, USA

[9]Molecular Biophysics and Integrated Bioimaging Division, Lawrence Berkeley National Laboratory, Berkeley, CA 94720, USA.

[10]Joint Program in Bioengineering, University of California, Berkeley/San Francisco, CA 94720, USA

[11]Environmental Genomics and Systems Biology Division, Lawrence Berkeley National Laboratory, Berkeley, CA 94720, USA.

[12]The Novo Nordisk Foundation Center for Biosustainability, Technical University of Denmark, Denmark

Abstract

Despite intensive study for 50 years, the biochemical and genetic links between lysine metabolism and central metabolism in *Pseudomonas putida* remain unresolved. To establish these biochemical links, we leveraged Random Barcode Transposon Sequencing (RB-TnSeq), a genome-wide assay measuring the fitness of thousands of genes in parallel, to identify multiple novel enzymes in both L- and D-lysine metabolism. We first describe three pathway enzymes that catabolize L-2-aminoadipate (L-2AA) to 2-ketoglutarate (2KG), connecting D-lysine to the TCA cycle. One of these enzymes, PP_5260, contains a DUF1338 domain, a family with no previously described biological function. Our work also identified the recently described CoA independent route of L-lysine degradation that metabolizes to succinate. We expanded on previous findings by demonstrating that glutarate hydroxylase CsiD is promiscuous in its 2-oxoacid selectivity. Proteomics of select pathway enzymes revealed that expression of catabolic genes is highly sensitive to particular pathway metabolites, implying intensive local and global regulation. This work demonstrates the utility of RB-TnSeq for discovering novel metabolic pathways in even well-studied bacteria, as well as a powerful tool for validating previous research.

Importance

P. putida lysine metabolism can produce multiple commodity chemicals, conferring great biotechnological value. Despite much research, connecting lysine catabolism to central metabolism in *P. putida* remained undefined. Herein we use Random Barcode Transposon Sequencing to fill in the gaps of lysine metabolism in *P. putida*. We describe a route of 2-oxoadipate (2OA) catabolism in bacteria, which utilizes DUF1338 containing protein PP_5260. Despite its prevalence in many domains of life, DUF1338 containing proteins had no known biochemical function. We demonstrate PP_5260 is a metalloenzyme which catalyzes an unusual 2OA to D-2HG decarboxylation. Our screen also identified a recently described novel glutarate metabolic pathway. We validate previous results, and expand the understanding of glutarate hydroxylase CsiD by showing can it use either 2OA or 2KG as a cosubstrate. Our work demonstrates biological novelty can be rapidly identified using unbiased experimental genetics, and that RB-TnSeq can be used to rapidly validate previous results.

Introduction

Pseudomonas putida is an ubiquitous saprophytic soil bacterium and is a model organism for bioremediation (1). Interest in utilizing *P. putida* KT2440 as a chassis organism for metabolic engineering has recently surged due to the existence of well-established genetic tools and its robust metabolism of aromatic compounds that resemble lignin hydrolysis products (2–4). As lignin valorization remains essential for the economic feasibility of cellulosic bioproducts, a nuanced and predictable understanding of *P. putida* metabolism is highly desirable (5).

Although its aromatic metabolism has garnered much attention, the lysine metabolism of *P. putida* has also been rigorously studied for over fifty years (6). An understanding of lysine metabolism has had biotechnological value, as it has been used to produce glutarate, 5-

69 aminovalerate (5AVA), as well as valerolactam in *P. putida* and in the other bacteria (7–10). Our
70 current understanding of lysine catabolism however, remains incomplete. In particular, the
71 connection between D-lysine metabolism and central metabolism in *P. putida* is unclear and has
72 not been fully characterized.

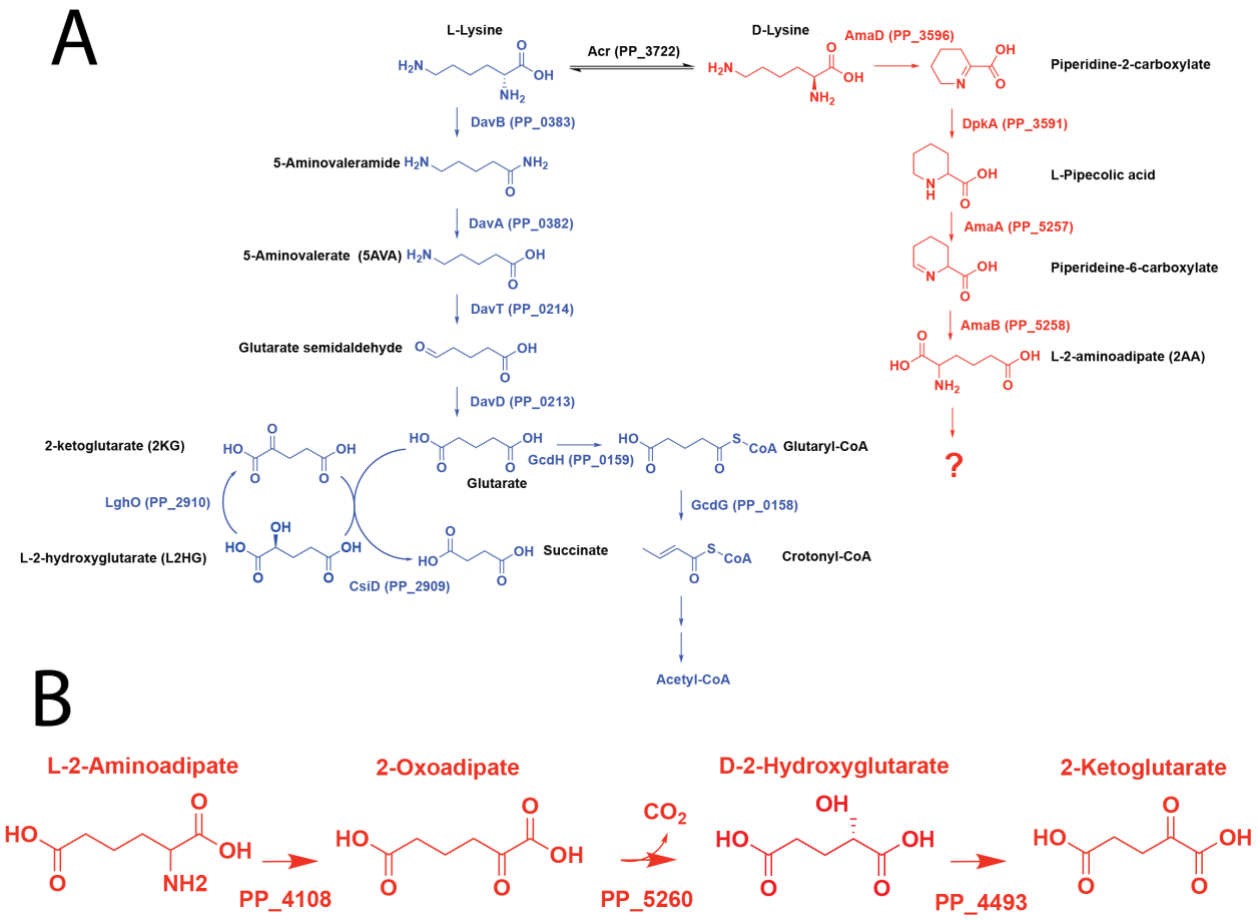

Figure S1**: Metabolic pathways of lysine catabolism in *P. putida* KT2440**. A) L-lysine metabolic pathway is shown in blue, while the known steps of D-lysine metabolism are shown in red. B) Proposed route of 2AA metabolism in *P. putida*.

73 *P. putida* employs bifucating pathways to catabolize lysine, separately metabolizing the
74 L- and D-isomers (Figure S1a) (11). The L-lysine degradation pathway proceeds to glutarate,
75 which can then be either be degraded to acetyl-CoA via a glutaryl-CoA intermediate, or to

76 succinate without a CoA bound intermediate (Figure S1a) (9). The final steps of D-lysine
77 catabolism remain more elusive. The initial steps of D-lysine catabolism are well described, but
78 the genetic basis stops at 2AA (12). Furthermore, ^{13}C labeling experiments by Revelles et al.
79 demonstrated a putative metabolic connection between the D- and L-lysine pathways at 2AA
80 (11). Subsequent steps to central carbon metabolism have never been fully validated. (6, 11–13).
81 Given the importance of lysine metabolism, and recent availability of high-throughput genetic
82 tools, we sought to identify the missing steps in D-lysine metabolism that have remained despite
83 50 years of research.

84 Random barcode transposon sequencing (RB-TnSeq) is a genome-wide approach that
85 measures the importance of each gene to growth (or fitness) in a massively parallel assay (14).
86 RB-TnSeq can identify phenotypes for thousands of previously uncharacterized genes (14, 15),
87 including the levulinic acid degradation pathway in *P. putida* KT2440 (16). In this study, we
88 applied RB-TnSeq to uncover multiple novel genes implicated in L- and D-lysine metabolism in
89 *P. putida*. We first describe a three enzyme route connecting L-2AA to 2KG (Figure S1B).
90 Within this pathway, D-lysine metabolism connects to central metabolism through a 2HG
91 intermediate, which is directly produced from 2OA in a reaction catalyzed by a DUF1338-
92 containing protein. This protein family, widely distributed across many domains of life,
93 previously had no known function. Subsequently, we further characterize the glutarate
94 hydroxylase CsiD, by demonstrating its 2-oxoacid promiscuity during the hydroxylation of
95 glutarate. Finally, we show the expression of all newly discovered enzymes changes significantly
96 in response to specific metabolites within the two catabolic pathways.

97 **Results**

98 Identification of lysine catabolism genes via RB-TnSeq

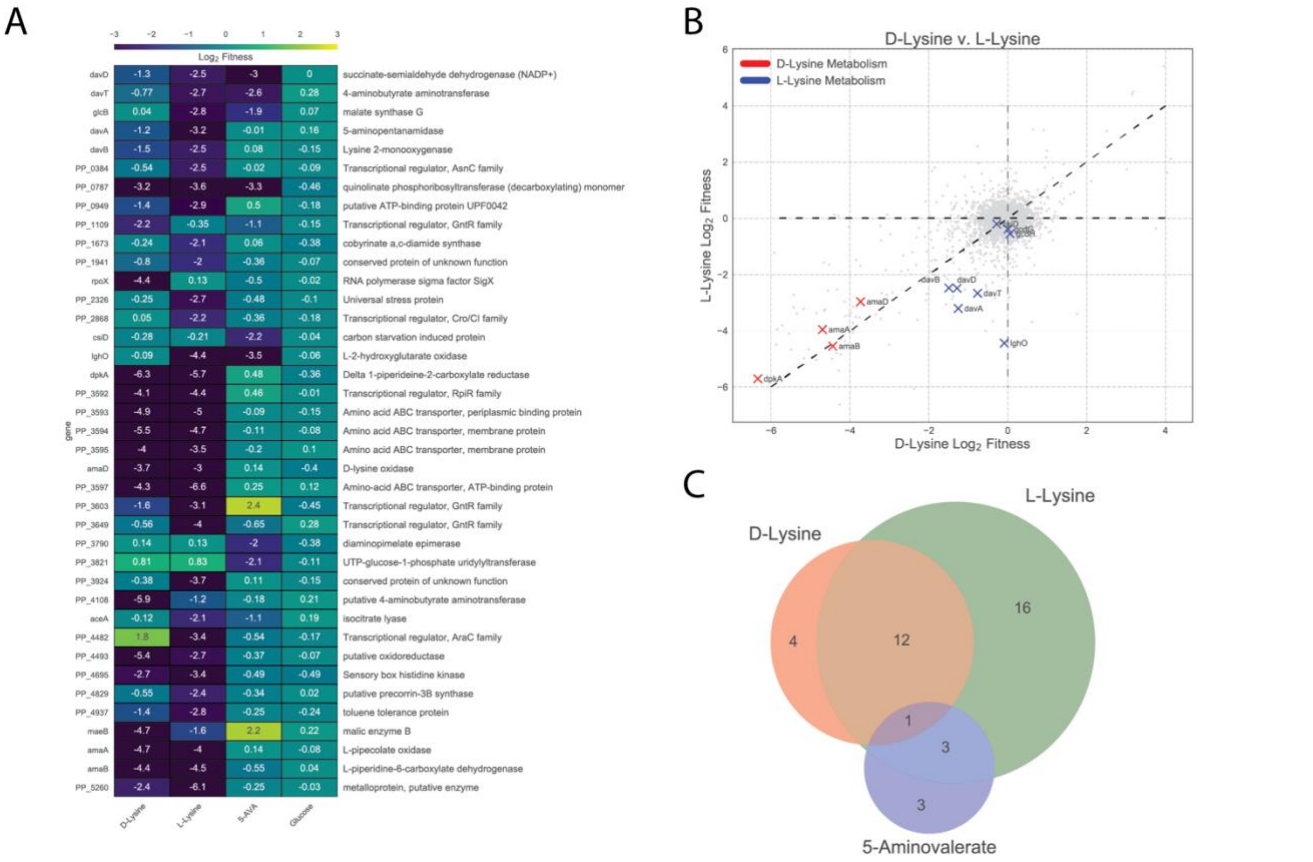

Figure 1: **Results of RB-TnSeq screen**. A) Genes that showed less than -2 $\log_2$ fitness on either D-lysine, L-lysine, or 5AVA but showed no less than -0.5 $\log_2$ fitness defect when grown on glucose. B) Plot of genome wide fitness values of libraries grown on either L-lysine or D-lysine. Genes encoding for enzymes known to be involved in D-lysine metabolism are shown in red, while those known to be involved in L-lysine metabolism are shown in blue. C) Venn diagram of genes with significant fitness defects when grown on either D-lysine, L-lysine, or 5AVA.

To identify mutants defective in lysine catabolism in *P. putida* KT2440, an RB-TnSeq library of this bacterium (16) was grown on minimal medium supplemented with either D-lysine or L-lysine as the sole carbon source. To evaluate whether D-lysine metabolism was required for the metabolism of other downstream metabolites of L-lysine, the library was also grown on 5AVA. As a control, we also grew the library on glucose. Fitness was calculated as the $\log_2$ ratio of strain and gene abundance at the end of selective growth relative to initial abundance (14).

Fitness profiling revealed 39 genes with significant fitness values of less than -2 for 5AVA, D-lysine, or L-lysine, and no less than -0.5 fitness for glucose (Figure 1a, Supplementary Table 1). Within this set, 10 of the 12 known lysine degradation genes were identified, with the exception of the two enzymes in the CoA-dependent route of glutarate degradation (*gcdH* and *gcdG*), which both had significant fitness values ($t < -4$) but whose fitness was greater than -2. Instead, we identified the recently-characterized genes involved in the CoA independent pathway (*csiD* and *lghO*) (9).

The fitness data corroborated previous work showing a functional D-lysine pathway is required for L-lysine catabolism (6, 11). None of the known L-lysine catabolic genes showed fitness defects for growth on D-lysine, but transposon insertions in all previously-identified D-lysine genes showed negative fitness scores when grown on L-lysine (Figure 1b). No known D-lysine catabolic enzymes showed fitness defects when grown on 5AVA, suggesting the D-lysine dependence of L-lysine catabolism may only occur for early catabolic steps (Figure 1c).

In addition to catabolic enzymes, lysine transporters and multiple transcriptional regulators were identified (Figure 1a). The putative lysine amino acid ABC transporter system (PP_3593, PP_3394, and PP_3395) showed significant fitness defects when grown with either isomer of lysine. Some of the transcriptional regulators were located near known catabolic or transport enzymes (PP_0384, PP_3592, and PP_3603), while others were not clustered with any obviously related genes (PP_1109, PP_2868, PP_3649, and PP_4482). Two known global regulators were identified in our screen: *cbrA* (PP_4695), a histidine kinase sensor that showed fitness defects on both lysine isomers, and the alternative sigma factor *rpoX* (PP_2088) which only had fitness defects when grown on D-lysine.

Additionally there were 15 genes which, when disrupted, displayed fitness advantages greater than 2 on 5AVA, D-lysine, or L-lysine and less than 0.5 fitness when grown on glucose. This positive fitness value indicates these mutations confer a competitive advantage compared to other strains when grown on these carbon sources. Most striking amongst these genes were the sigma factor *rpoS* and the LPS export system (PP_1778/9), which when disrupted, both displayed fitness benefits on all three non-glucose carbon sources (Figure S2).

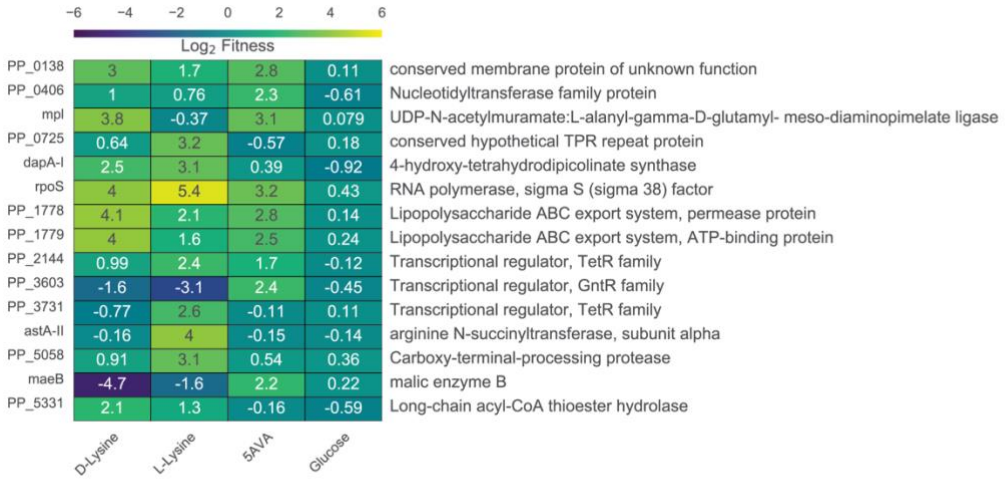

Figure S2: Results of RB-TnSeq screen. A) Genes that showed great than 2 log2 fitness on either D-lysine, L-lysine, or 5AVA but showed no less than 0.5 log2 fitness defect when grown on glucose.

Only one gene (PP_0787, a quinolinate phosphoribosyltransferase) showed fitness defects on all three non-glucose carbon sources (Figure 1c). However, disruption of PP_0787 also showed a significant fitness defect when grown on levulinic acid, suggesting it is unlikely to be uniquely important to lysine metabolism (16). Only 3 genes shared fitness defects between 5AVA and L-lysine (*davT*, *davD*, and *lghO*), all of which have been previously implicated in 5AVA metabolism (Figure 1c) (9).

141 PP_4108 is a L-2AA aminotransferase

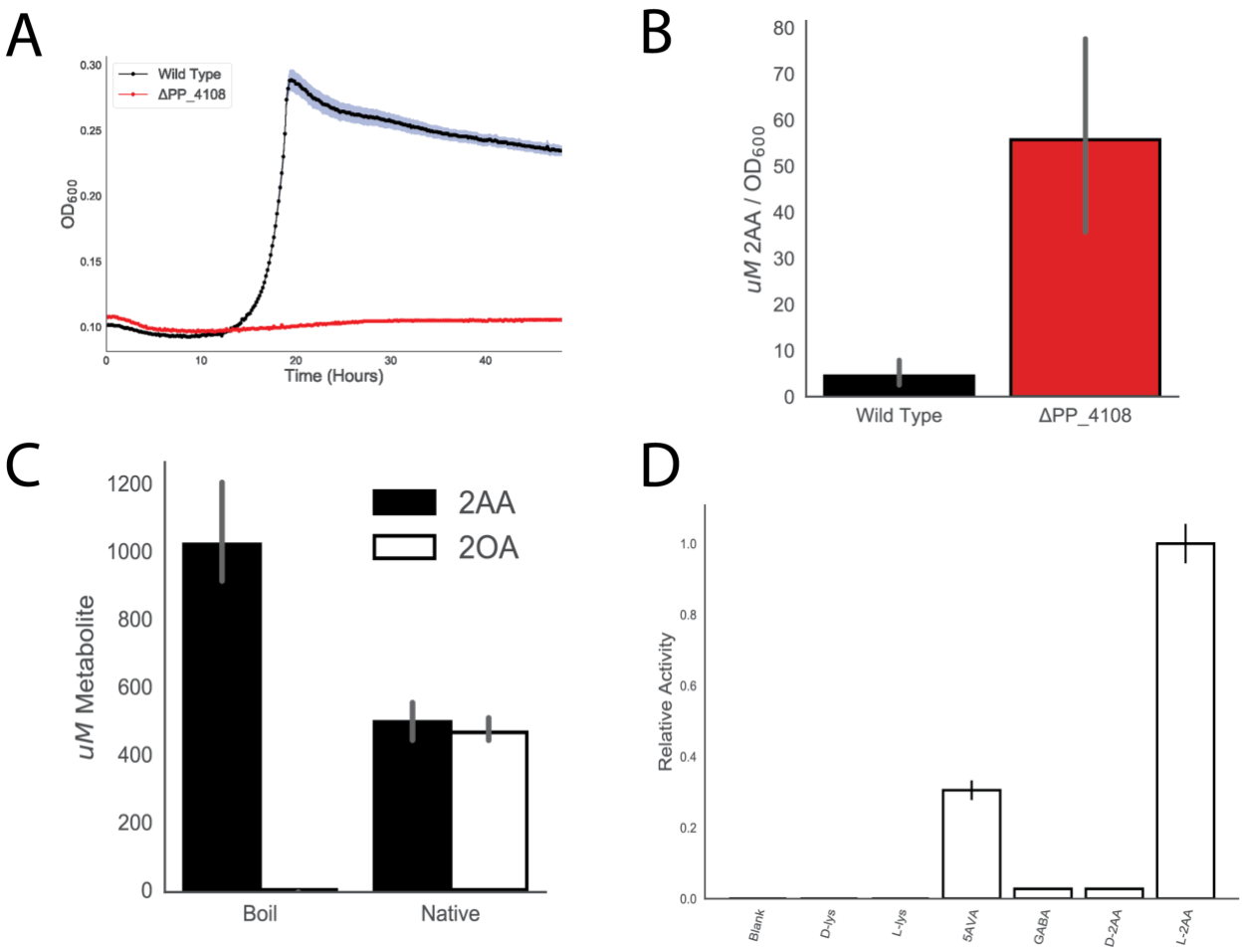

Figure 2: **Identification of PP_4108 as a L-2AA aminotransferase**. A) Growth of wild-type KT2440 and PP_4108 mutant on 2AA as a sole carbon source. Shaded area represents 95% confidence interval (CI), n=3. B) *In vivo* accumulation of 2AA in wild-type KT2440 and a PP_4108 mutant after 12 hours of growth on minimal medium supplemented with 10 mM glucose and 10 mM D-lysine. Bars represent $1og_{10}$ transformed spectral counts, error bars show 95% CI, n=3. C) *In vitro* transamination reactions of PP_4108 with 2KG as an amino acceptor. Bars represent µM metabolite concentration of either 2OA (black) or 2AA (white) in either boiled or native protein reactions. Error bars show 95% CI, n=3. D) *In vitro* transaminations of PP_4108 incubated with different possible amino donors and 2KG as acceptor. Bars represent relative activity of enzyme standardized to L-2AA after 16 hour incubation. Error bars show standard deviation, n=2.

In humans and other animals, L-lysine degradation proceeds through a 2AA intermediate, which a transaminase converts to 2OA (9, 11, 17). Yet, no such transaminase has been identified in *P. putida*. We identified a candidate aminotransferase, PP_4108, for which gene inactivation showed a significant growth defect on D-lysine (-5.9) and a relatively minor defect on L-lysine (-1.2). To corroborate our RB-TnSeq fitness data, we constructed a deletion mutant of PP_4108 that failed to grow in a plate reader assay on 10 mM DL-2AA (Figure 2a). The mutant showed a severe growth defect on 10 mM D-lysine and an increased lag time when grown on 10 mM L-lysine (Figure S3).

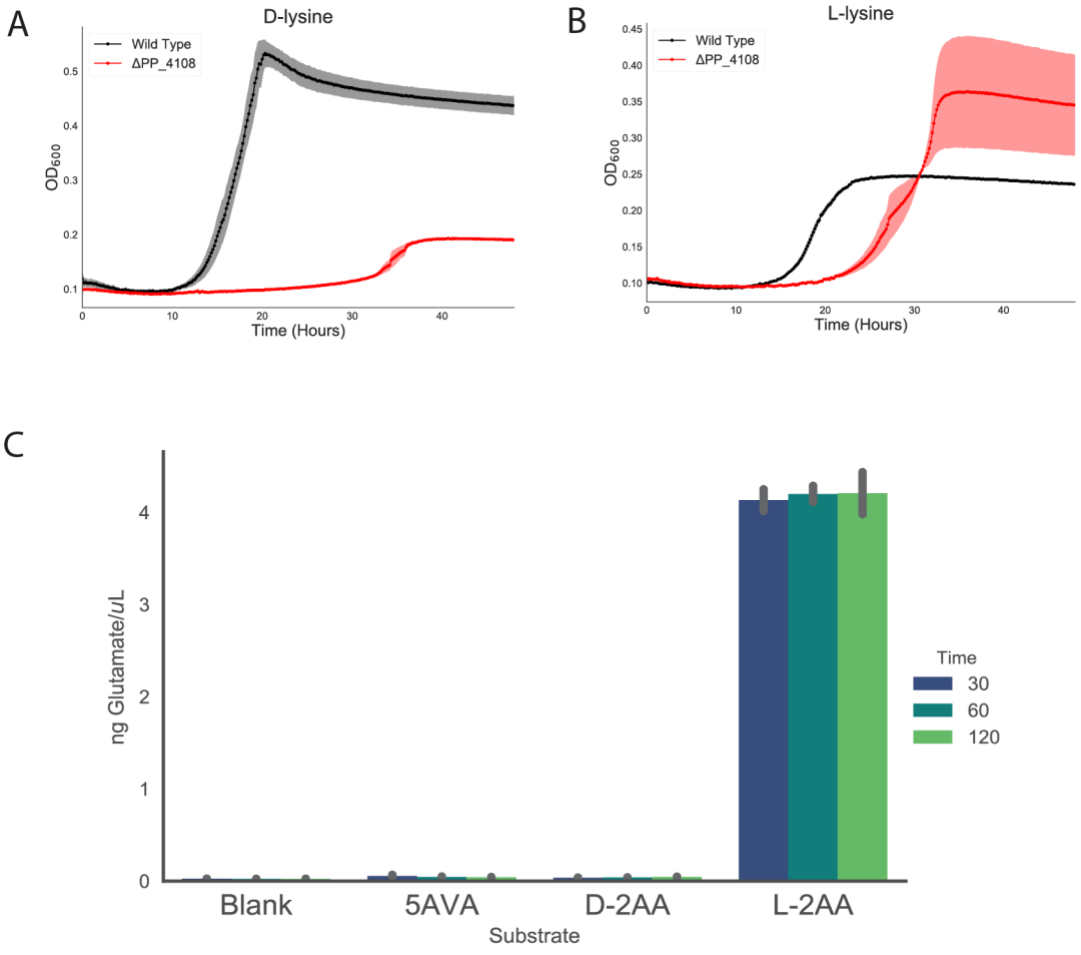

Figure S3**: Growth of PP_4108 mutants on lysine**. A) Growth of wild-type KT2440 and PP_4108 mutant on D-lysine as a sole carbon source. Shaded area represents 95% CI, n=3. B) Growth of wild-type KT2440 and PP_4108

mutant on L-lysine as a sole carbon source. Shaded area represents 95% CI, n=3. C) Colorimetric glutamate formation time course of PP_4108. Error bars are standard deviation of n=2.

To further validate this hypothesis, the ΔPP_4108 strain was subjected to metabolomics analysis to monitor the accumulation of its expected substrate, 2AA, when grown on glucose and D-lysine. After 12 hours of growth on minimal media supplemented with 10 mM each of glucose and D-lysine, the PP_4108 deletion strain showed a 6.3-fold increase (p = 0.00016) in normalized intracellular 2AA concentration compared to WT (Figure 2b). Next PP_4108 was expressed and purified from *E. coli* for biochemical characterization. After purified enzyme incubation with DL-2AA, 2KG, and pyridoxal phosphate (PLP) for 16 hours, the reaction mixture was analyzed with LC-TOF. The expected product, 2OA, was detected in the enzymatic reaction but not in a boiled enzyme control, confirming PP_4108 as a transaminase that converts 2AA to 2OA (Figure 2c). As many transaminases have broad substrate specificity (18), we also probed the substrate range of PP_4108 using a colorimetric assay for glutamate, a stoichiometric product of the transamination reaction (Figure 2d). The enzyme was most active on L-2AA, and only showed 2.8% relative activity (p = 0.0057) on its enantiomer, D-2AA. This specificity for the L-2AA isomer may explain why only 50% of the DL-2AA was transformed in the previous experiment (Figure 2c). No activity was observed on either lysine isomer; however, the enzyme had slight activity towards 4-aminobutyrate/γ-aminobutyrate (GABA) (2.8% relative activity, p = 0.0057) and moderate activity on 5AVA (30.5% relative activity, p = 0.0139). Over shorter time scales PP_4108 had no activity on any substrate expect L-2AA (Figure S3c). These results suggest *P. putida* KT2440 metabolizes D-lysine to L-2AA, which is then converted to 2OA by the transaminase PP_4108.

PP_5260 is a novel DUF1338 family enzyme that catalyzes the conversion of 2OA to 2HG

Early work proposed 2OA is converted to 2KG via a 2HG intermediate (13, 19), while later results suggested a direct conversion of 2OA to glutarate (11). Either route likely requires a decarboxylation of 2OA, so we initially searched for decarboxylases within our dataset. Our fitness data on either lysine isomer revealed no obvious decarboxylases or enzymes likely to contain a thiamine pyrophosphate (TPP) cofactor, which are commonly employed by decarboxylases. However, a gene near other D-lysine catabolic genes in the *P. putida* genome, PP_5260, showed a significant fitness defect. A ΔPP_5260 strain was unable to grow on either

isomer of lysine verifying its importance in lysine degradation (Figure 3a).

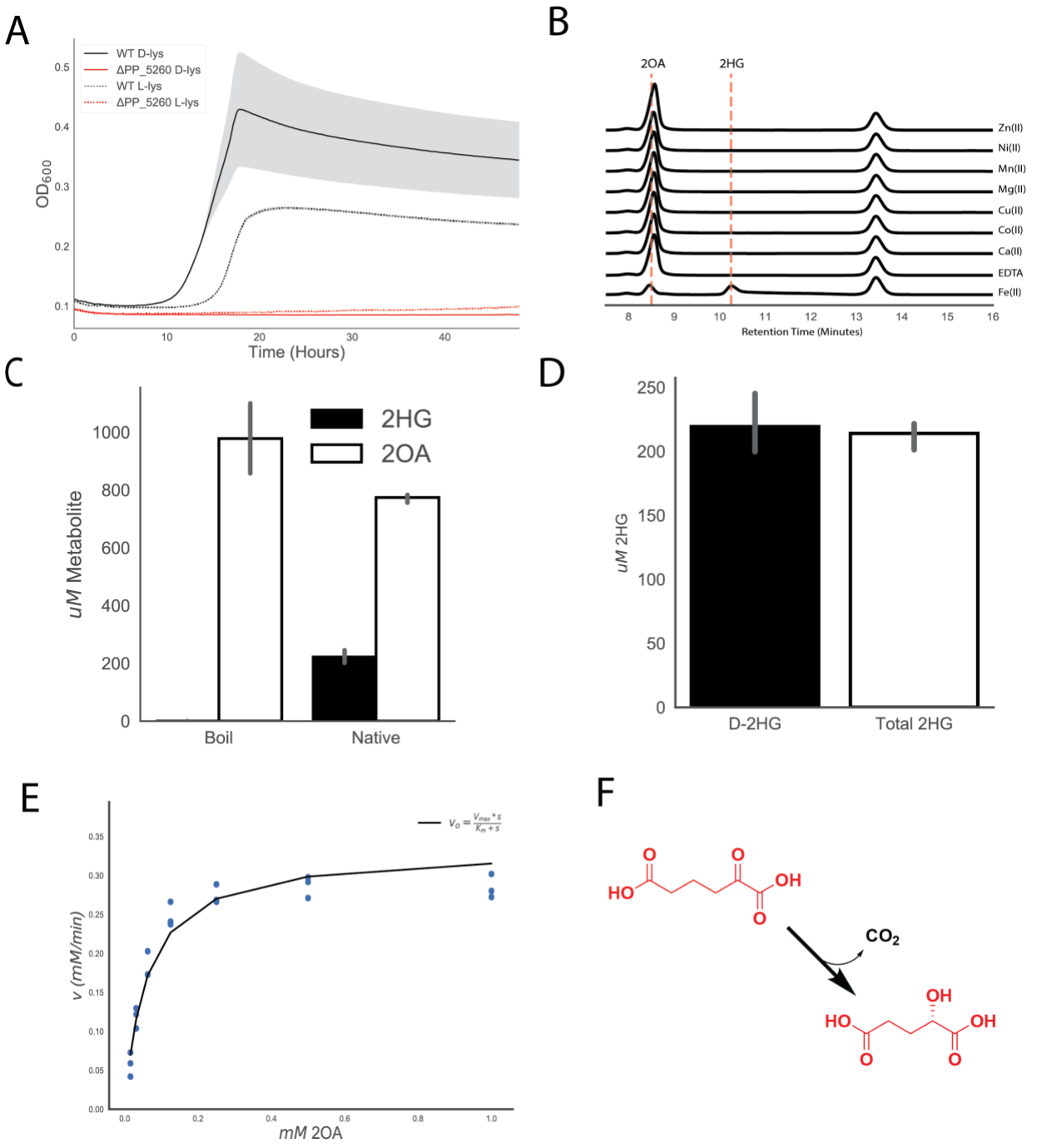

Figure 3: **Identification of ydcJ (PP_5260) as a 2OA decarboxylase/hydroxylase.** A) Growth of wild-type (black) and PP_5260 mutant (red) on D-lysine (line) or L-lysine (dashed line) as a sole carbon source. Shaded area represents 95% CI, n=3. B) HPLC traces of *in vitro* reactions run with apo PP_5260 with exogenous metals added at 50 µM. Retention times for 2OA and 2HG are shown by vertical dashed lines.

Metal or EDTA control is indicated to the right of traces. C) *In vitro* assay of 2OA conversion to 2HG by purified PP_5260 protein analysed via LC-TOF. 2OG in white, 2HG in black. D) *In vitro* assay of purified PP_5260 protein with 2OA as substrate. Black bar represents concentration of D-2HG measured by enzyme coupled assay. White bar represents total 2HG concentration as measured by LC-TOF. Error bars represent 95% CI, n=3. E) Initial velocity of reaction catalyzed by PP_5260 as a function of 2OA concentration. Blue dots represent individual measurements, while the black fit line shows a Michaelis-Menten fit. F) Chemical reaction catalyzed by PP_5260, 2OA is decarboxylated to D-2HG.

PP_5260 belongs to the DUF1338 protein family (http://pfam.xfam.org/family/PF07063). Although several unpublished crystal structures of DUF1338 domain containing proteins have been deposited into the Protein Data Bank, their biological function remains elusive. However, these structures combined with protein sequence alignments suggest a putative metal binding site is conserved throughout the DUF1338 family. As we hypothesized PP_5260 serves as the missing decarboxylase in D-lysine metabolism, we purified the enzyme for biochemical analysis. Enzymatic activity on 2OA was probed and analyzed via LC-TOF. After incubation of 2OA with PP_5260, we observed a ~92% (p=0.00034) reduction in the abundance of 2OA, whereas no 2OA was consumed in a boiled enzyme control or enzyme treated with EDTA confirming it to be a metalloenzyme (Figure S4a). Initially we believed the product would be either glutarate or glutarate semialdehyde, however neither of these was detected in the reaction. Early biochemical work suggested 2HG as a potential intermediate in pipecolate metabolism (19), and when the enzymatic product was compared to a racemic 2HG standard they shared the same mass, retention time and mass-to-charge ratio (Figure S4b), as well identical isotopic distributions of

[M-H] peaks in the mass spectra (Figure S4c).

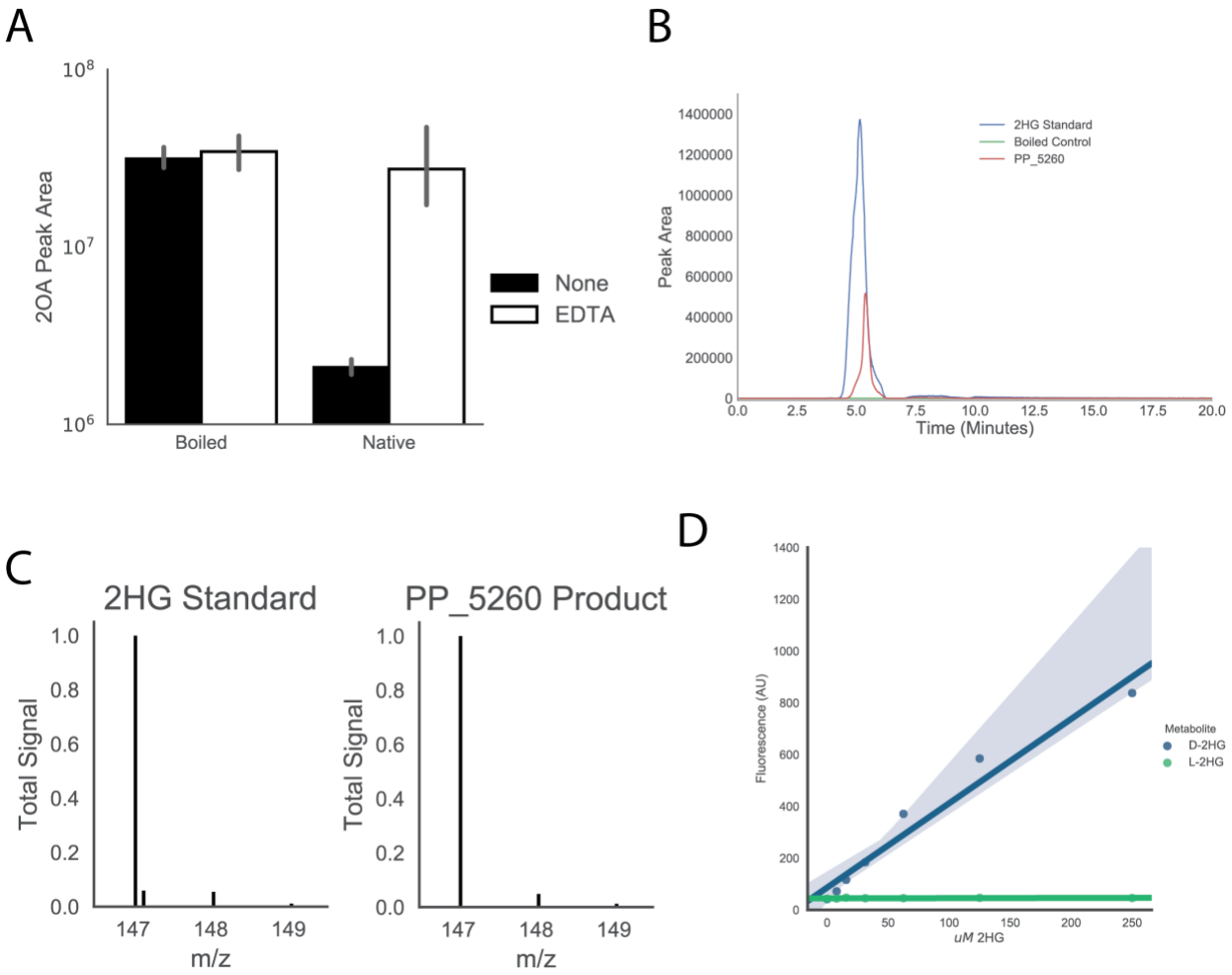

Figure S4: **Characterization of PP_5260**. A) In vitro reactions of boiled or native PP_5260 incubated with 2OA with 50 µM EDTA (white), or without EDTA (black). Bars represent $1og_{10}$ transformed spectral counts, errors bars represent 95% CI, n=3 B) E LC-TOF analysis of a 2HG standard, and products of PP_5260 incubated with 2OA, and boiled control. C) Mass spectra of 2HG standard and product of PP_5260 in vitro reaction. D) Standard curves of D-2HG and L-2HG using a D-2HG specific enzymatic detection assay. Shaded areas represent 95% CI, n=3.

To identify the metal cofactor, the enzyme was dialyzed against EDTA to remove metals, and individual divalent metals were added back. Only the addition of Fe(II) restored enzymatic activity as measured by HPLC (Figure 3b). Subsequent reactions quenched after 5 minutes

showed 200 uM of 2HG formed and 800 uM 2OA remaining, demonstrating 1:1 2OA to 2HG reaction stoichiometry (Figure 3c). Whether the product of the PP_5260 reaction is either L-2HG or D-2HG is critical to understanding the eventual fate of D-lysine, as *lghO* is specific for L-2HG (Figure S1a). An enzyme coupled assay specific for the detection of D-2HG was used to assess the stereochemistry of the PP_5260 product. Standard curves of D-2HG and L-2HG showed that the assay was only responsive to D-2HG (Figure S4d). The concentration of *in vitro* reactions of PP_5260 were then measured by both LC-TOF as well as the enzyme coupled assay, revealing all 2HG as the D-isomer (Figure 3d).

Kinetic parameters of PP_5260 were determined using an enzyme-coupled assay to spectrophotometrically measure CO_2 evolution via NADH oxidation (20). PP_5260 displayed a V_{max} of 0.33 mM/min (+/- 0.08 mM), a K_m of 0.06 mM (+/- 0.03 mM), and a K_{cat} of 330 m^{-1} using 2OA as a substrate. Taken together these results reveal that PP_5260 is novel Fe(II) dependent decarboxylase that converts 2OA to D-2HG (Figure 3f), a chemical reaction not previously observed in nature.

DUF1338 proteins are a widely distributed enzyme family with a putative conserved role in amino acid catabolism

After functional characterization of PP_5260, we use phylogenomics to propagate the annotation and further explore the biological role of DUF1338 proteins found in other organisms. We found that DUF1338 proteins are widely distributed across the tree of life, with homologs of PP_5260 found in plants and green algae (22), fungi, and bacteria, though they were not found in animals or archaea (Figure 4a). Homologs are widely distributed amongst bacteria, with the Firmicutes being a notable exception. PP_5260 homologs within the plant group Streptophyta, as well as bacterial groups Actinobacteria, Cyanobacteria, and Bacteroidetes formed monophyletic

clades, while homologs from other taxonomic groups were not monophyletic (Figure 4a). DUF1338 homologs are found in bacteria important to biotechnology (*Corynebacterium glutamicum*), the environment (*Nostoc puncitforme*), and medicine (*Yersinia pestis*, *Mycobacterium tuberculosis*, *Burkholderia pseudomallei*).

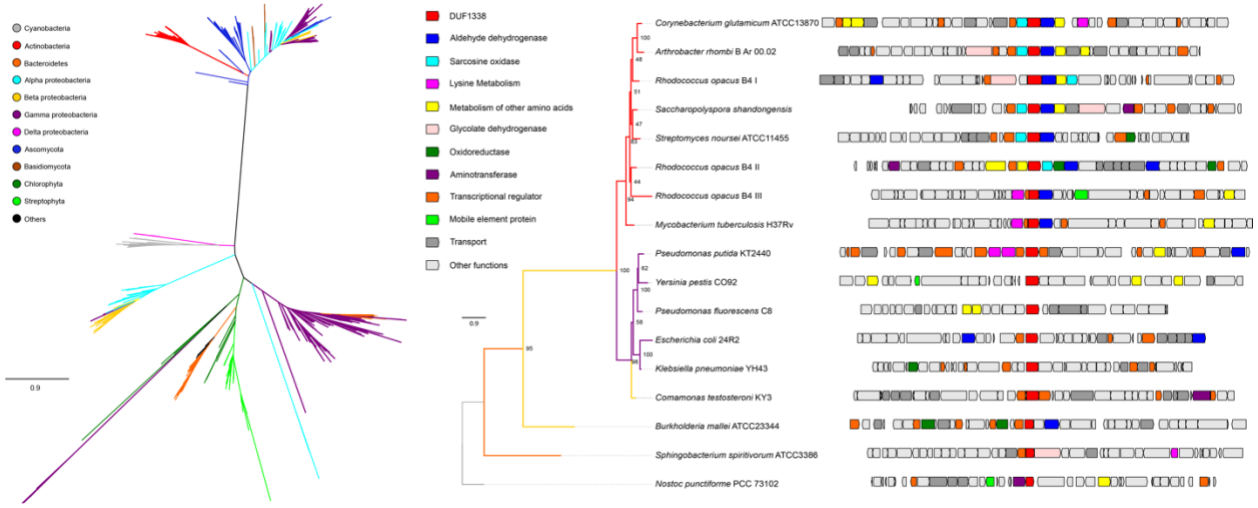

Figure 4: **Phylogenomics of the DUF1338 enzyme family**. A) Phylogenetic relationships among DUF1338 homologs and their distribution among major phyla. Branches in the tree are colored by phylum. DUF1338 is found in most bacterial phyla as well as in plants and fungi. Non-monophyletic clades suggest pervasive horizontal gene transfer events in the family. B) Phylogenomics of selected DUF1338 homologs in bacteria. The phylogeny in the left shows the phylogenetic relationships between selected homologs, the branches have been colored according to their adscription to a given phylum and the support values are shown at the nodes. The boxes in the right represent the gene neighborhood for each homolog. The genes have been colored to represent their annotated functions.

Publicly available fitness data show both *Pseudomonas fluorescens* FW300-N2C3 and *Sinorhizobium meliloti* PP_5260 homologs have L-lysine specific defects when interrupted (15). Genomic contexts within other bacteria suggest many DUF1338-containing enzymes may be involved in lysine or other amino acid metabolism (Figure 4b). Within the Actinobacteria DUF1338 homologs are often found adjacent to sarcosine oxidases, aldehyde dehydrogenases,

and transaminases implying an additional catabolic amino acid function. In both the oleaginous bacterium *Rhodococcus opacus* B4 and *M. tuberculosis*, DUF1338 homologs are found next to predicted L-lysine aminotransferases, suggesting an ancestral homolog functioned in lysine catabolism. Interestingly, the *R. opacus* B4 genome has three DUF1338 homologs, only one of which contains genes predicted to be specific to lysine catabolism. The other two gene neighborhoods are similar in their functional content, mainly differing by containing an oxidoreductase or glycolate dehydrogenase, either of which may perform the same biochemical function. In Alphaproteobacteria, Betaproteobacteria, and Cyanobacteria, the presence of aldehyde dehydrogenases, oxidoreductases, glycolate dehydrogenases, and aminotransferases implies a metabolic function similar to PP_5260.

PP_4493 putatively oxidizes D-2HG to 2KG and connects D-lysine to central metabolism

In the CoA independent route of glutarate metabolism, LghO oxidizes L-2HG to 2KG, however this enzyme is highly specific towards the L-2HG isomer and showed no fitness defect on D-lysine in our RB-TnSeq data (Figure S1a). A putative FAD-dependent and 4Fe-4S cluster-containing glycolate dehydrogenase, PP_4493, did show fitness defects on both D-lysine and L-lysine (fitness scores of -5.4 and -2.7 respectively) (Figure 1a). Glycolate dehydrogenases are members of a larger family of enzymes that oxidize the alcohol group of an alpha-hydroxyacid to their corresponding alpha-ketoacid (Figure 5a). Therefore, we hypothesized PP_4493 could potentially oxidize a similar 2-hydroxyacid, 2HG, to the corresponding alpha-ketoacid, 2KG. Moreover, many PP_5260 homologs were located next to or near putatively annotated glycolate dehydrogenases in other bacteria, underscoring their potential metabolic link (Figure 4b). To confirm these hypotheses, we again constructed a deletion strain, *P. putida* ΔPP_4493, which could not grow on D-lysine as a sole carbon source (Figure 5b), and showed attenuated growth

on L-lysine (Figure S5). Furthermore, when grown on 10 mM glucose and 10 mM D-lysine the mutant accumulated ~500 uM 2HG normalized to optical density, whereas wild type *P. putida* did not accumulate any detectable 2HG (Figure 5c). Subsequent analysis of accumulated 2HG via a D-2HG specific detection kit revealed that this accumulated 2HG was indeed D-2HG (Figure 5c). These data and the conserved function and genomic context of glycolate dehydrogenases strongly suggest PP_4493 catalyzes the last step of L-2AA metabolism, oxidizing D-2HG to 2KG (Figure S1b).

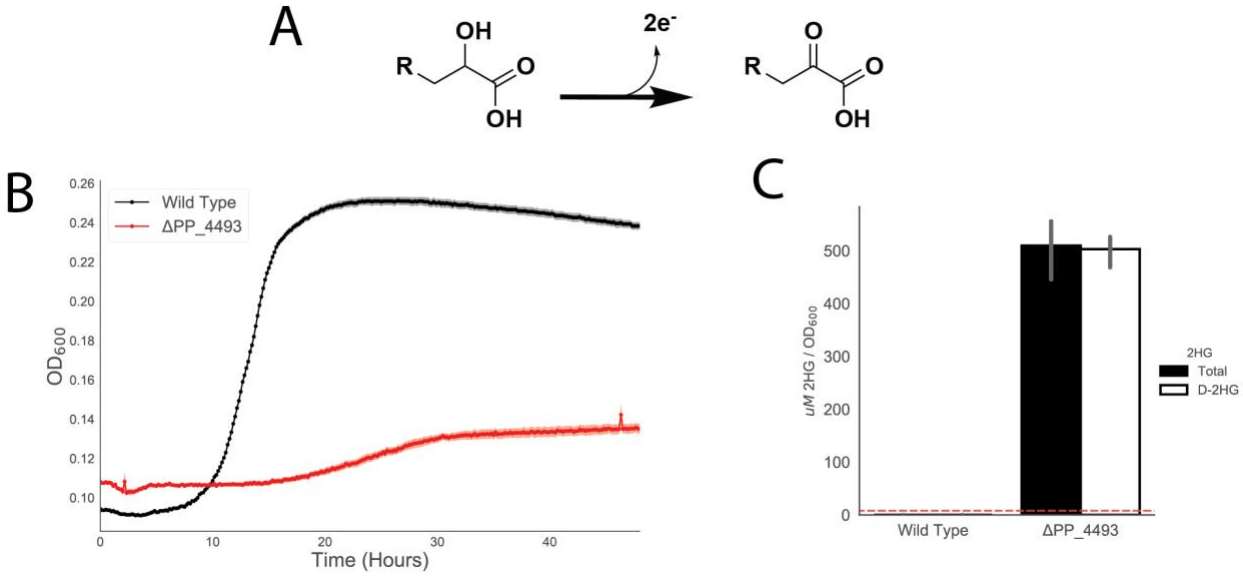

Figure 5: **Identification of PP_4493 as a putative D-2HG dehydrogenase**. A) General chemical reaction of a dehydrogenase converting a 2-hydroxyacid to a 2-ketoacid B) Growth of *P. putida* KT2440 and PP_4108 mutant on D-lysine as a sole carbon source. Shaded area represents 95% CI, n=3. C) *In vivo* accumulation of 2HG in wild-type KT2440 and a PP_4108 mutant after 12 hours of growth on minimal medium supplemented with 10 mM glucose and 10 mM D-lysine. White bar represents concentration of D-2HG measured by enzyme coupled assay. Black bar represent total 2HG concentration as measured by LC-TOF. Red line represents limit of detection of enzyme coupled assay for D-2HG. Bars represent $1og_{10}$ transformed spectral counts, error bars show 95% CI, n=3.

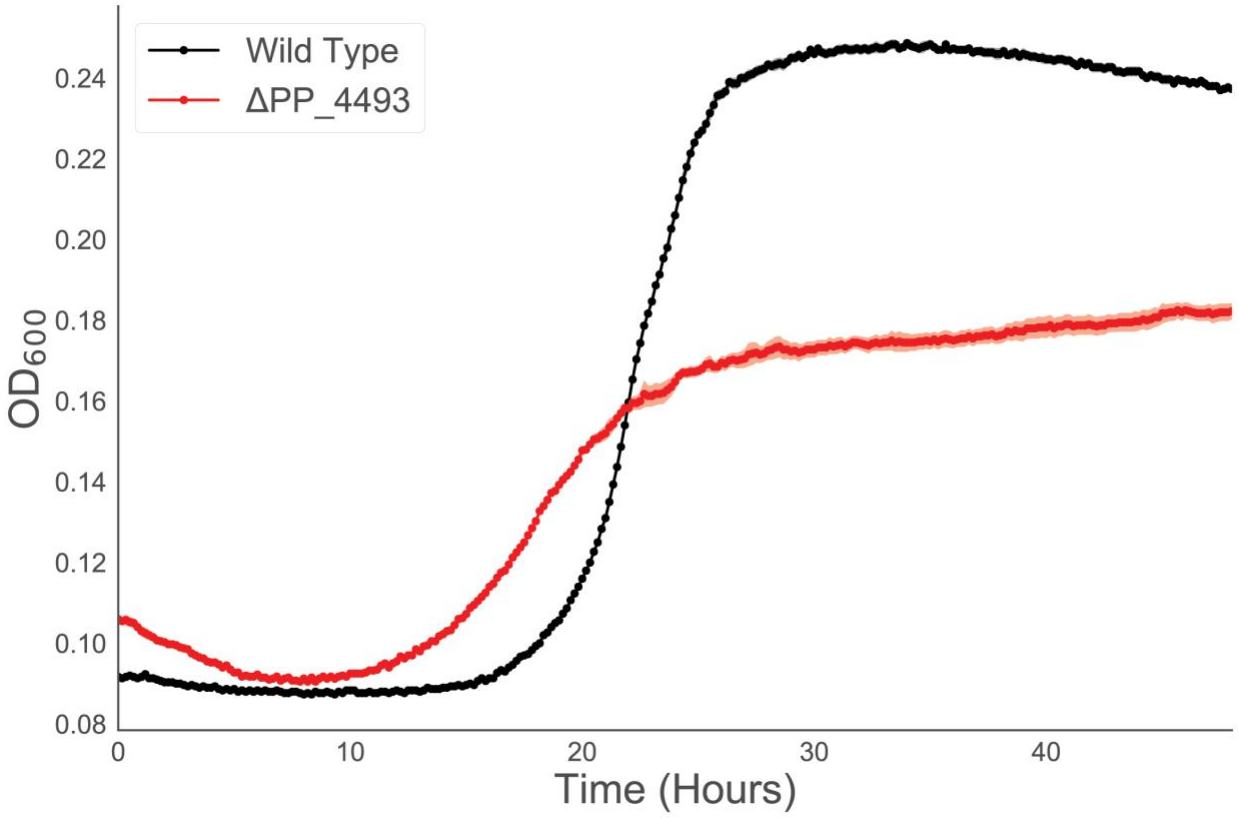

Figure S5**: Growth of PP_4493 mutant on L-lysine.** Growth of wild-type KT2440 and PP_4493 mutant on L-lysine as a sole carbon source. Shaded area represents 95% CI, n=3

CsiD is highly specific for glutarate hydroxylation but promiscuous in 2-oxoacid selectivity

During the initial preparation of this manuscript, Zhang et al. discovered a novel pathway of glutarate metabolism in *P. putida (9)*. They describe a cyclic reaction cascade wherein a novel 2KG-dependent non-heme Fe(II) oxygenase, PP_2909 (CsiD), hydroxylates glutarate to form 2HG and succinate using 2KG as a cosubstrate. PP_2910 (LghO), a putative L-2HG oxidase, then subsequently converts L-2HG to 2KG, regenerating the 2KG consumed in the initial reaction. These reactions result in the net incorporation of succinate into central metabolism (Figure S1). Our fitness results of the library grown on 5AVA also identified both *csiD* and *lghO*, in addition to the two enzymes from the CoA-dependent glutarate pathway, glutaryl-CoA

ligase (*gcdG*) and glutaryl-CoA dehydrogenase (*gcdH*), mutants of which showed mild fitness defects when grown on 5AVA (Figure 6a). We also purified *csiD* and confirmed it hydroxylates glutarate in a 2KG-dependent manner (Figure S6a). HPLC analysis demonstrated that as glutarate was consumed, equimolar quantities of succinate and L-2HG were produced (Figure S6b). Additionally, a *csiD* deletion mutant showed increased lag time when grown on either L-lysine or 5AVA. By deleting the glutaryl-CoA ligase *gcdG*, and disrupting the CoA-dependent glutarate pathway, we completely prevented growth on 5AVA or L-lysine (Figure S6c). These results are in agreement with those found with Zhang et al (9).

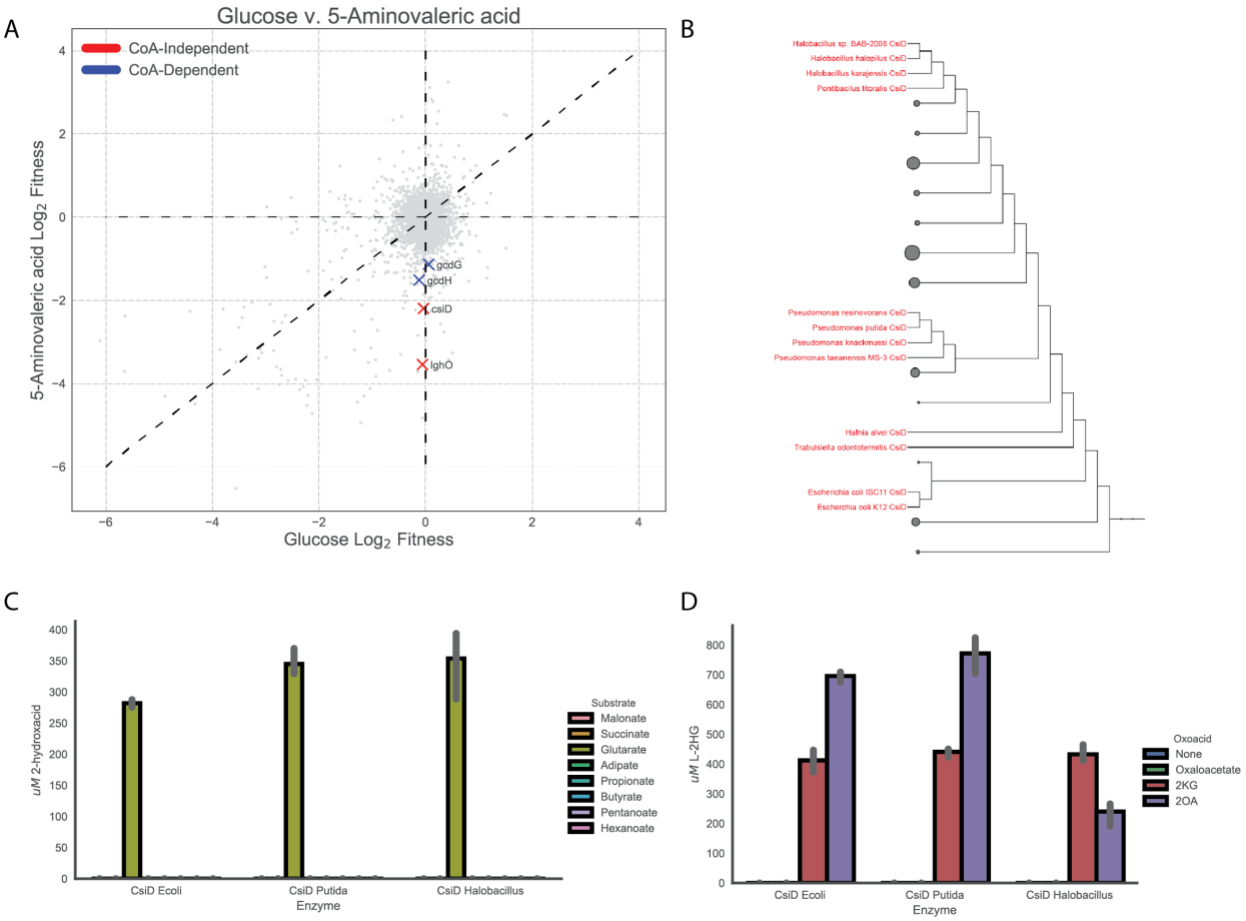

Figure 6: **Role of CsiD in *P. putida* lysine metabolism**. A) Plot of genome wide fitness values of libraries

grown on either 5AVA or glucose. CoA-dependent glutarate degradation genes are shown in red, while those known to be involved succinate producing metabolism are shown in blue. B) Phylogenetic tree of bacterial CsiD homologs. Homologs used in *in vitro* assays are highlighted in red. C) *in vitro* reactions of CsiD with different substrates using 2KG as a 2-oxoacid. Bars show peak area of 2-hydroxyacid, error bars show 95% CI, n=3. D) *In vitro* reactions of CsiD homologs with different 2-oxoacids. Bars represent spectral counts of L-2HG. Error bars show 95% CI, n=3.

Because non-heme Fe(II) oxidases can be promiscuous with respect to the 2-oxoacid cosubstrate (21, 22), we evaluated the 2-oxoacid specificity of CsiD. First, we evaluated the hydroxyl acceptor substrate specificity of CsiD family proteins by purifying two additional homologs from *E. coli* and a halophilic bacterium, *Halobacillus* sp. BAB-2008 (Figure 6b). We probed the activity of the homologs against a panel of 3 to 6 carbon fatty acids and diacids in the presence of 2KG, and found only glutarate served as a hydroxylation substrate (Figure 6c). These results are consistent with the work recently reported by Zhang *et al (9)* and further suggests the specificity of CsiD homologs is conserved across phyla. Although extremely specific for the hydroxylation substrate, all three CsiD homologs could utilize both 2OA and 2KG, but not oxaloacetate, as a cosubstrate for L-2HG formation (Figure 6d). The coproduct of the reaction using 2OA as a 2-oxoacid would be glutarate, rather than succinate. This result is particularly interesting as it provides a possible mechanism for the previously observed metabolic link between D-lysine and L-lysine catabolism. Growth defects observed in a ΔPP_2909 ΔPP_0158 double mutant grown on D-lysine also support this hypothesis (Figure S7a).

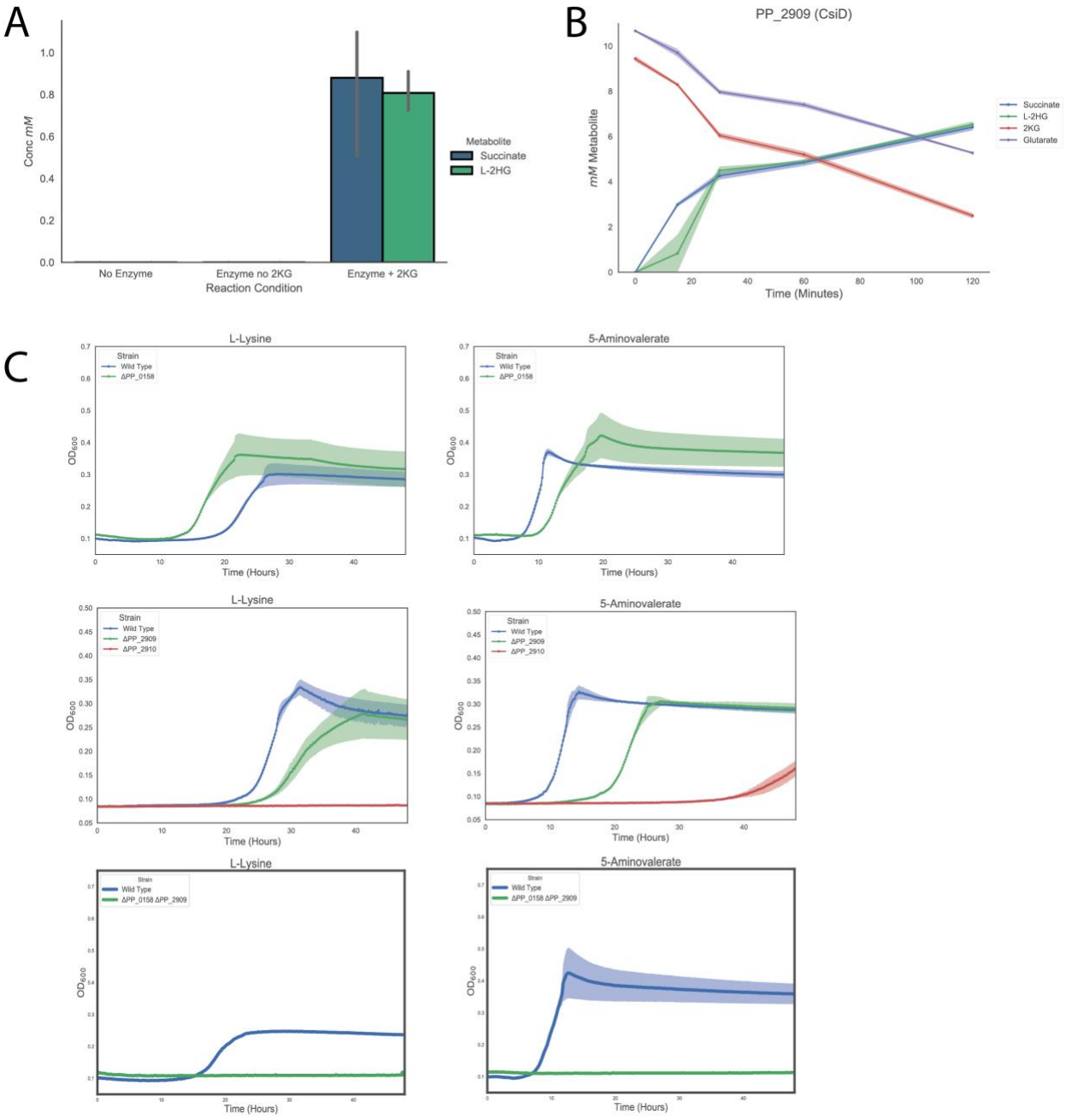

Figure S6: **Characterization of PP_2909 (CsiD) in *P. putida***. A) In vitro reactions of PP_2909. Bars show mM of either succinate (blue), or 2HG (green) formed by boiled enzyme control, no 2KG control, or native enzyme with 2KG added. Errors bars show 95% CI, n=3. B) Time course in vitro reaction of PP_2909. Plot shows 2HG, 2KG, succinate, and glutarate overtime. Shaded region shows 95% CI, n=3. C) Growth curves of wild-type KT2440, PP_0158, PP_2909, PP_2910, or PP_2909/PP_0158 double mutants grown on either L-lysine (left column), or

5AVA (right column). Shaded region shows 95% CI, n=3.

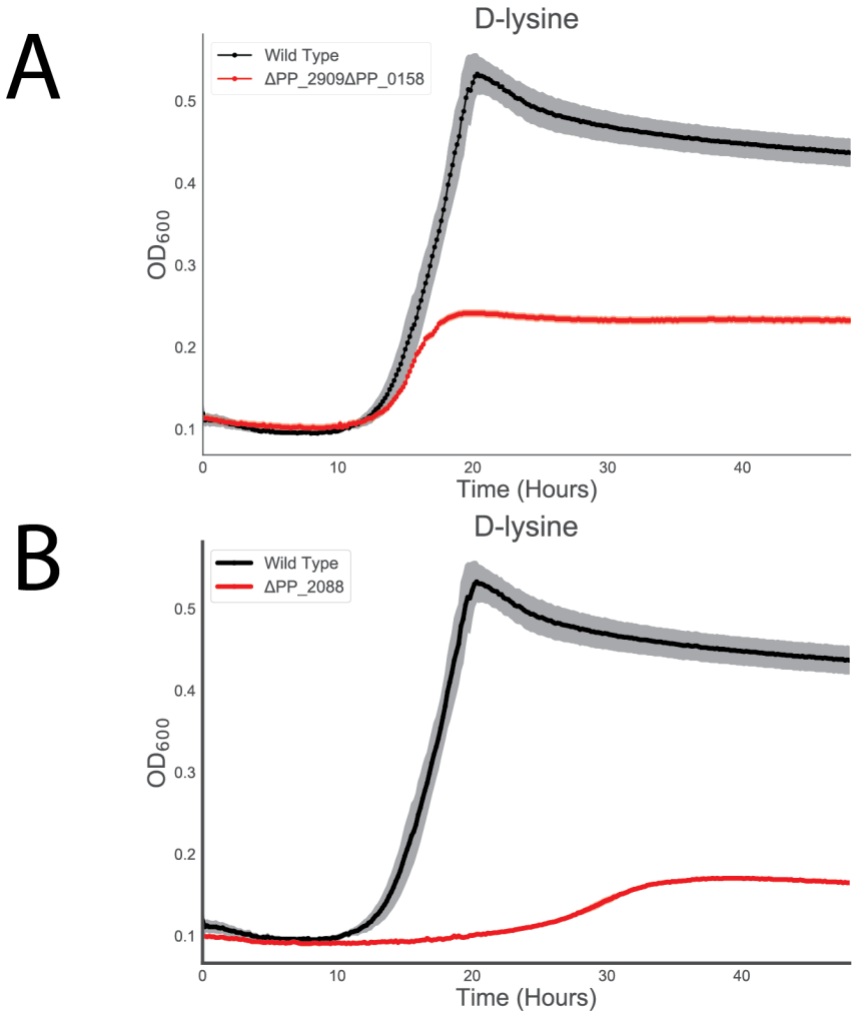

Figure S7: **Growth of PP_2909/PP_0158 and PP_2088 mutants on D-lysine**. A) Growth of wild-type KT2440 and PP_2909/PP_0158 mutant on D-lysine as a sole carbon source. Shaded area represents 95% CI, n=3. A) Growth of wild-type KT2440 and PP_2088 mutant on D-lysine as a sole carbon source. Shaded area represents 95% CI, n=3.

Expression of lysine metabolic proteins is responsive to pathway metabolites

Multiple studies have demonstrated the expression of lysine catabolic genes is upregulated in the presence of pathway metabolites (9, 12, 23). To investigate the regulation of the newly-discovered lysine catabolic enzymes from this study, wild-type *P. putida* KT2440 was grown in minimal media on glucose or a single lysine metabolite (e.g. D-lysine, L-lysine, 5AVA,

2AA, or glutarate) as a sole carbon source until cultures reached an OD_{600} of 1.0. We then quantified the relative abundance of D- and L-lysine catabolic proteins via targeted proteomics (Figure 7). For each protein, all pairwise statistical comparisons of different carbon sources can be found in Supplemental Table 2. All five D-lysine pathway proteins measured (AmaA (PP_5257), AmaB (PP_5258), PP_4108, YdcJ (PP_5260), and YdiJ (PP_4493)) were upregulated when grown on L-lysine, D-lysine or 2AA compared to the glucose control. Neither 5AVA nor glutarate significantly induced expression of any measured D-lysine proteins. Of all the targeted proteins, the three identified in this study that directly degrade 2AA were most strongly induced by 2AA. Somewhat surprisingly, we also found the two enzymes involved in 2AA formation, AmaA and AmaB, were also more highly expressed in the presence of 2AA suggesting the possible involvement of a global regulator. An interesting finding from our initial screen showed sigma factor RpoX (PP_2088) to be required for fitness on D-lysine (Figure 1a). Deletion mutants of *rpoX* were severely attenuated in their ability to grown on D-lysine as a sole carbon source (Figure S7b). Further work will be necessary to examine complex regulatory network that controls D-lysine metabolism.

The initial two enzymes from L-lysine metabolism, DavA and DavB, were most highly expressed in the presence of L-lysine, but also significantly with D-lysine. As previously observed, DavT and DavD were most strongly upregulated on 5AVA, moderately upregulated on L-lysine, and to a lesser extent D-lysine. The induction of LhgO and CsiD was highest when grown on glutarate, although these proteins were also moderately upregulated by 5AVA and L-lysine. By comparison, PP_0159 (GcdG) expression in the presence of glutarate was stimulated to a lesser extent than LhgO and CsiD expression; in addition, GcdG was slightly upregulated on 5AVA and L-lysine.

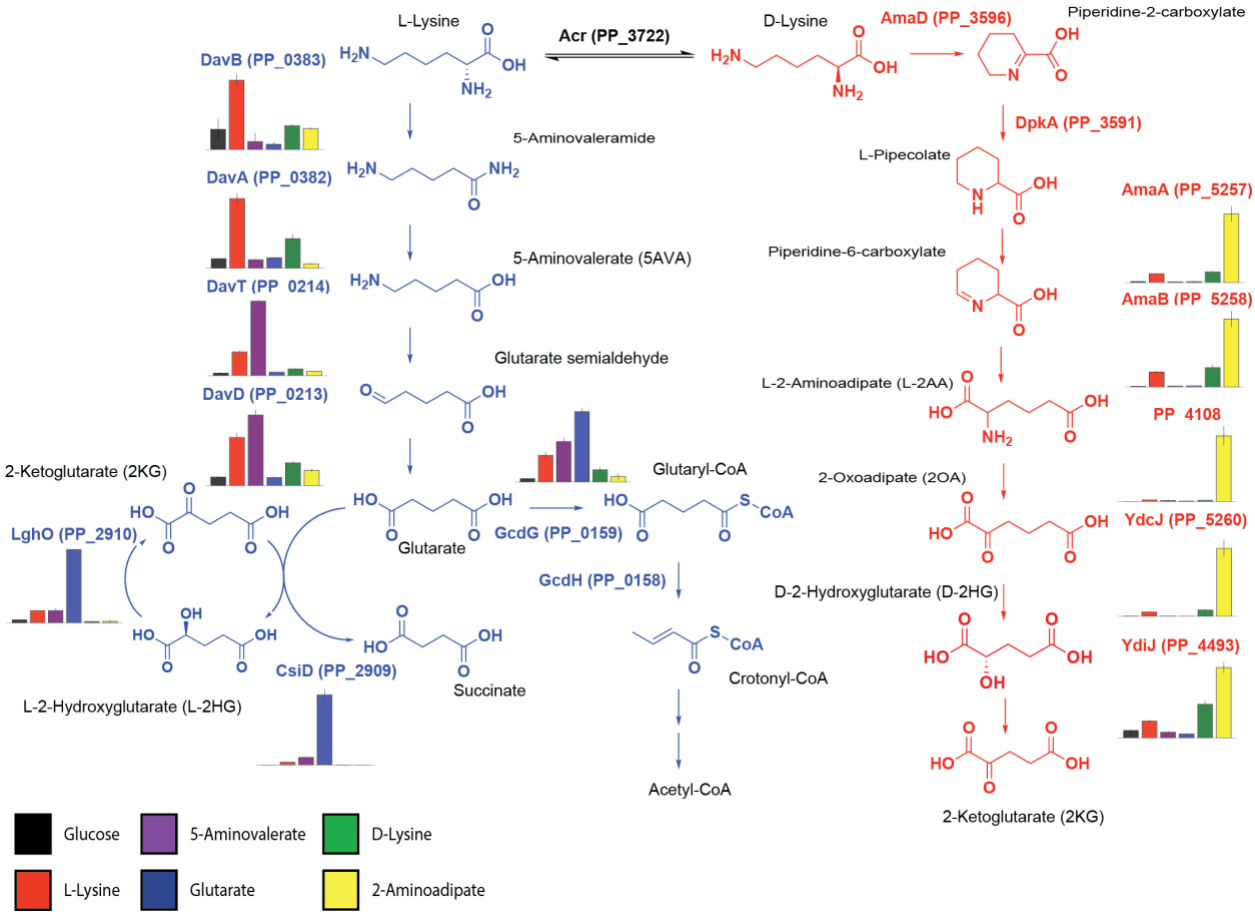

Figure 7: **Expression of lysine degradation pathways in response to different lysine metabolites**. Relative abundance of selected lysine degradation enzymes expressed in wild-type KT2440 in response to different carbon sources. Bars show spectral counts of proteins after 36 hours of growth on 10 mM glucose (black), 5AVA (purple), D-lysine (green), L-lysine (red), glutarate (blue), or 2AA (yellow). Error bars show 95% CI, n=3.

Discussion

Despite intensive study, a complete biochemical and genetic understanding of D-lysine catabolism in *P. putida* has remained elusive. A 2OA degradation pathway has been extensively characterized in mammals, because of its implications in human disease (24). In the mammalian pathway, L-lysine is metabolized to 2OA and eventually converted to acetyl-CoA via a glutaryl-

CoA intermediate (24). However, this pathway has not been observed in bacteria. Previous work suggested 2OA is either converted via decarboxylation to glutarate or through several enzymatic steps to 2HG, yet none of these studies conclusively demonstrated a genetic and biochemical basis for these hypotheses (11, 19, 25). In this work we demonstrate plausible biochemical routes to account for both of these previously hypothesized pathways.

The first route, catalyzed by the DUF1338-containing metalloenzyme PP_5260, involves the direct conversion of 2OA to D-2HG. The formation of the D-2HG isomer by PP_5260 maintains stereochemical separation from the L-2HG formed by L-lysine degradation, thus requiring the dehydrogenase PP_4493 rather than the L-2HG specific oxidase *lghO*. This transformation seemingly involves two separate reactions: a decarboxylation and a hydroxylation. Hydroxymandelate synthase has been shown to catalyze a similar enzymatic reaction, via an intramolecular oxidative decarboxylation similar to 2KG dependent Fe(II) oxidases (26). PP_5260 is also a Fe(II) dependent decarboxylase, and the two share similar Kcat values for their given substrates (330 m^{-1} for PP_5260 and 270 m^{-1} for hydroxymandelate synthase) (27). Though PP_5260 and hydroxymandelate synthase share little sequence homology, this enzyme may give us insight into the molecular mechanism of DUF1338 enzymes. We have given PP_5260 the tentative title of 2-hydroxyglutarate synthase (*hglS*) until further mechanistic studies (currently underway in our group) are completed and a more accurate enzyme name can be assigned.

In bacteria, homologs of PP_5260 appear widely distributed with their genomic contexts suggesting functions both within and beyond lysine metabolism. Genomic contexts in other bacteria, particularly *Actinobacteria*, suggest these homologs may be involved in other amino acid catabolic pathways. Unfortunately, there is scant evidence for homologous function in

model organisms. For example, although DUF1338 proteins are present in other *Ascomycota*, there is no homolog in *Saccharomyces cerevisiae*. Interestingly, the *E. coli* homolog of PP_5260 is located next to a potential glucans biosynthesis gene: Glucans biosynthesis protein D (28). Another DUF1338-containing protein from rice has been characterized and was implicated in starch granule formation (29). These results suggest DUF1338 proteins could play a role in sugar metabolism.

Recently Zhang *et al*. thoroughly characterized a CoA independent glutarate catabolism route ending at succinate involving the Fe(II) dependent oxygenase CsiD (9). Our RB-TnSeq screening convergently uncovered this pathway, and our biochemical and physiological results fully corroborate their findings. While both works show multiple CsiD homologs from divergent bacteria are highly specific towards glutarate as a hydroxyl acceptor, all three homologs we tested showed promiscuous activity toward 2-oxoacid cosubstrates. The ability of the *P. putida* CsiD to utilize 2OA as a cosubstrate is particularly interesting as it may directly connect L- and D-lysine metabolism. The promiscuity of CsiD may explain earlier studies which reported glutarate formation from D-lysine (11). Further studies involving labelled substrates may help elucidate the potential link between the two pathways. While CsiD plays a clear role in L-lysine metabolism in *P. putida*, its role in other organisms remains a mystery. In *E. coli*, RpoS controls the expression of CsiD, but *rpoS* mutants showed fitness benefits on all three lysine metabolites tested in our RB-TnSeq data (30). Recent work has shown that *E. coli* also uses CsiD to metabolize lysine, suggesting a possible conserved role for this pathway across bacteria (31).

Work presented here and previous reports have shown expression of both lysine catabolism pathways are highly responsive to their respective metabolites. While this metabolism appears highly coordinated, the genes themselves are dispersed across the genome, with both

448 PP_4018, and PP_4493 found outside of operons, and relatively distant from other lysine
449 catabolic genes. At least two global regulators appeared to be important to lysine metabolism
450 based on our Rb-TnSeq data, *cbrA* (PP_4695) and *rpoX* (PP_2088). The two-component system
451 CbrAB has been implicated in catabolite repression and C/N balance in *P. aeruginosa*, with
452 mutants unable to grown on multiple amino acids (32). Further work in *P. putida* KT2440
453 showed the CbrAB system behaved similarly to that in *P. aeruginosa* (33). It would be
454 unsurprising if this regulator controls the expression of various genes within lysine catabolism;
455 more work into uncovering the regulon is warranted. RpoX on the other hand has been
456 implicated in osmotic tolerance in *P. aeruginosa* (34, 35). This is interesting as lysine
457 metabolism, and specifically pipecolate metabolism, has been associated with osmotic tolerance
458 across multiple bacteria (36). As a *rpoX* deletion mutant was unable to grow on D-lysine, these
459 results suggest D-lysine metabolism of *P. putida* may be involved in adaptation to saline or other
460 osmotically stressful environments.

461 An interesting question remains as to why *P. putida* maintains separate metabolic
462 pathways for D- and L-lysine, and why L-lysine metabolism seems dependent on the presence of
463 an intact D-lysine metabolism. Previously work has proposed that the D-lysine pathway may
464 provide a way of resolving a C/N imbalance that may occur when L-lysine is metabolized.
465 However we believe this is unlikely as both lysine degradation pathways contain one
466 deamination and one transamination reaction (11). Our fitness results indicate D-lysine
467 metabolism is dispensable for growing on 5AVA. This would suggest only the initial two steps
468 of L-lysine metabolism, the oxidation of lysine to 5-aminopentanamide by DavB and its
469 subsequent deamination to 5AVA by DavA are dependent on D-lysine catabolism. We propose
470 the adjacent AsnC family regulator PP_0384 likely responds to L-lysine as many proteins within

this family respond to amino acids including lysine (37, 38) and expression of these two enzymes is most responsive to L-lysine. To our knowledge there has been no rigorous characterization of the regulation of the *davAB* operon, nor of the biochemical activities of these two enzymes *in vitro*. Future studies to uncover the mechanistic regulation at the transcriptional and post-translational levels at these two steps may uncover the necessity of D-lysine dependency of the L-lysine catabolic pathway. Overall our work highlights the utility of global fitness profiling to discover novel, complex, metabolic pathways in even well-characterized bacteria.

Materials and Methods

Media, chemicals, and culture conditions

Routine bacterial cultures were grown in in Luria-Bertani (LB) Miller medium (BD Biosciences, USA). *E. coli* was grown at 37 °C, while *P. putida* was grown at 30 °C unless otherwise noted. When indicated, *P. putida* was grown on modified MOPS minimal medium (39). Cultures were supplemented with kanamycin (50 mg/L, Sigma Aldrich, USA), gentamicin (30 mg/L, Fisher Scientific, USA), or carbenicillin (100mg/L, Sigma Aldrich, USA), when indicated. D-2AA was purchased from Takara Bioscience (USA), all other compounds were purchased through Sigma Aldrich.

Strains and plasmids

All bacterial strains and plasmids used in this work are listed in Supplemental Table 1. All strains and plasmids created in this work are available through the public instance of the JBEI registry. (https://public-registry.jbei.org/folders/391). All plasmids were designed using Device Editor and Vector Editor software, while all primers used for the construction of plasmids were designed using j5 software (40–42). Synthetic DNA coding for the *Halobacillus* sp. BAB-2008 *csiD* homolog was purchased from Integrated DNA Technologies (IDT,

Coralville, IA). Plasmids were assembled via Gibson Assembly using standard protocols (43), or Golden Gate Assembly using standard protocols (44). Plasmids were routinely isolated using the Qiaprep Spin Miniprep kit (Qiagen, USA), and all primers were purchased from Integrated DNA Technologies (IDT, Coralville, IA).

Random barcode TnSeq experiments

P. putida RB-TnSeq library JBEI-1 was created by diluting a 1 mL aliquot of the previously described *P. putida* RB-TnSeq library (16) in 500 mL of LB media supplemented with kanamycin which was then grown to an OD_{600} of 0.5 and frozen as 1 mL aliquots after adding glycerol to a final concentration of 20% v/v. Libraries were stored at −80 °C until used. A 1 mL aliquot of *P. putida* RB-TnSeq library JBEI-1 was thawed on ice and diluted in 25 mL of LB supplemented with kanamycin. The culture was grown until it reached an OD_{600} of 0.5, at which point 3 1-mL aliquots were taken, pelleted, decanted, and then stored at −80 °C to use as a time zero control. The library was then washed once in MOPS minimal medium without any carbon source, and then diluted 1:50 into 10 mL MOPS minimal medium supplemented with either 10 mM glucose, 5AVA, D-lysine, or L-lysine. Cells were grown in 50 mL culture tubes for 48 hours at 30 °C shaking at 200 rpm. After growth 2 ml aliquots from the culture tubes were pelleted, decanted and frozen at −80 °C for barcode sequencing. We performed DNA barcode sequencing (BarSeq) as previously described (14, 16). The fitness of a strain is the normalized log2 ratio of barcode reads in the experimental sample to barcode reads in the time zero sample. The fitness of a gene is the weighted average of the strain fitness for insertions in the central 10–90% of the gene. The gene fitness values are normalized so the typical gene has a fitness of zero. The primary statistic *t*-value is of the form of fitness divided by the estimated variance across different mutants of the same gene. Statistic *t*-values of $>|4|$ were considered significant. All

517 experiments described herein pass the quality metrics described previously unless noted
518 otherwise. All fitness data in this work is publically available at http://fit.genomics.lbl.gov.

519 Construction of deletion mutants

520 Deletion mutants in *P. putida* were constructed by homologous recombination and *sacB*
521 counterselection using the allelic exchange vector pMQ30 (45). Briefly, homology fragments
522 ranging from 1 kbp to 2 kbp up- and downstream of the target gene, including the start and stop
523 codons respectively, were cloned into pMQ30. An exception to these design parameters was
524 plasmid pMQ-PP_5260 which maintained an additional 21 nt at the 5' end of the gene in
525 addition to the stop codon. Plasmids were then transformed via electroporation into *E. coli* S17
526 and then mated into *P. putida* via conjugation. Transconjugants were selected for on LB agar
527 plates supplemented with gentamicin 30 mg/mL, and chloramphenicol 30 mg/mL.
528 Transconjugants were then grown overnight on LB media also supplemented with 30 mg/mL
529 gentamicin, and 30 mg/mL chloramphenicol, and then plated on LB agar with no NaCl
530 supplemented with 10% w/v sucrose. Putative deletions were restreaked on LB agar with no
531 NaCl supplemented with 10% w/v sucrose, and then were screened via PCR with primers
532 flanking the target gene to confirm gene deletion.

533 Plate based growth assays

534 Growth studies of bacterial strains were conducted a microplate reader kinetic assays.
535 Overnight cultures were inoculated into 10 mL of LB medium from single colonies, and grown
536 at 30 °C. These cultures were then washed twice with MOPS minimal media without any added
537 carbon and diluted 1:100 into 500 uL of MOPS medium with 10 mM of a carbon source in 48-

538 well plates (Falcon, 353072). Plates were sealed with a gas-permeable microplate adhesive film
539 (VWR, USA), and then optical density was monitored for 48 hours in an Biotek Synergy 4 plate
540 reader (BioTek, USA) at 30 °C with fast continuous shaking. Optical density was measured at
541 600 nm and all OD_{600} measurements are reported without pathlength corrections.

542 Expression and purification of proteins

543 A 5 mL overnight culture of *E. coli* BL21 (DE3) containing the expression plasmid was
544 used to inoculate a 500 mL culture of LB. Cells were grown at 37 ºC to an OD_{600} of 0.6 then
545 induced with isopropyl β-D-1-thiogalactopyranoside to a final concentration of 1 mM. The
546 temperature was lowered to 30 ºC and cells were allowed to express for 18 hours before being
547 harvested via centrifugation. Cell pellets were stored at -80 ºC until purification. For purification,
548 cell pellets were resuspended in lysis buffer (50 mM sodium phosphate, 300 mM sodium
549 chloride, 10 mM imidazole, 8% glycerol, pH 7.5) and sonicated to lyse cells. Insolubles were
550 pelleted via centrifugation (30 minutes at 40,000xg). The supernatant was applied to a fritted
551 column containing Ni-NTA resin (Qiagen, USA) which had been pre-equilibrated with several
552 column volumes of lysis buffer. The resin was washed with lysis buffer containing 50 mM
553 imidazole, then the protein was eluted using a step-wise gradient of lysis buffer containing
554 increasing imidazole concentrations (100 mM, 200 mM, and 400 mM). Fractions were collected
555 and analyzed via SDS-PAGE. Purified protein was dialyzed overnight at 4 ˚C against 50 mM
556 HEPES pH 7.5, 5% glycerol.

557 CsiD *in vitro* assays

558 The activity of purified CsiD homologs was analyzed in 100 µL reaction mixtures
559 containing 50 mM HEPES (pH 7), 5 mM glutarate, 5 mM 2KG, 25 µM $FeSO_4$, 0.1 mM
560 ascorbate, and 0.5 mM dithiothreitol. For negative control reactions, each respective reaction

component was omitted. To initiate reactions, CsiD was added to a final concentration of 7 µM. For the no enzyme control, CsiD was denatured at 98 °C for 10 minutes prior to addition to the reaction mix. Reactions were allowed to proceed at 22 °C for 3 hours. Products were analyzed via LC-TOF method 3 after quenching via the addition of acetonitrile and methanol for a final ACN:H_2O:MeOH ratio of 6:3:1 To analyze products from substrate range as well 2-oxoacid specificity experiments, reactions were measured via LC-TOF method 1.

Transamination assays

To determine product formation via PP_4108, assays were conducted in 50 mM HEPES (pH 7.5), with 5 mM 2KG, 0.1 mM PLP, and 5 mM of substrate, and 10 µM of purified enzyme or boiled enzyme control in 100µL volumes. Reactions were incubated at 30 °C for 16 hours and quenched via the addition of ACN and MeOH for a final ACN:H_2O:MeOH ratio of 6:3:1 for LC-TOF method 3. To determine substrate specificity reactions were set up at 75 µL scale and carried out at 30°C for up to 16 hours before freezing. For analysis, reactions were diluted 15-fold in water and assessed by a colorimetric assay for glutamate (Sigma MAK004) in 96-well format via a SpectraMax M4 plate reader (Molecular Devices, USA).

PP_5260 *in vitro* assays

The activity of PP_5260 was initially assessed in 50 mM HEPES, with 5 mM 2OA as substrate and 10 µM purified enzyme or boiled enzyme control. Reactions were incubated for 16 hours at 30 °C. To test the necessity of metal cofactors EDTA was added to a final concentration of 50 µM. Reactions and quenched via the addition of ACN and methanol MeOH for a final ACN:H_2O:MeOH ratio of 6:3:1 for LC-TOF analysis method 3, or with an equal volume of ice-cold methanol for HPLC analysis and LC-TOF method 2.

583 To determine the metal cofactor, after purification over Ni-NTA resin the protein was
584 concentrated and dialyzed overnight against 50mM HEPES, 100mM NaCl, pH 7.5. To generate
585 apo-enzyme, the protein was then dialyzed four times at a protein:dialysis buffer ratio of 1:300
586 against the same buffer containing 5mM EDTA in order to remove any bound metal. The
587 enzyme was dialyzed once more against buffer without EDTA overnight in order to remove any
588 remaining chelating reagent. The apo-enzyme was then assayed in the presence of 50 µM of a
589 variety of potential metal cofactors in 50 mM HEPES with 10 mM 2OA as substrate and 10 µM
590 purified enzyme. Reactions were incubated for 30 minutes at 30 ^{o}C and activity was assessed via
591 HPLC.

592 Determination of enzyme stoichiometry was assessed in 50 mM HEPES, 50 µM $FeCl_2$,
593 with 1 mM 2OA as substrate and 0.1 µM purified enzyme or boiled enzyme control. Reactions
594 were incubated for 5 minutes at 30 ^{o}C and then quenched with an equal volume of ice-cold
595 methanol then quantified with LC-TOF method 2.

596 Enzyme coupled decarboxylation assays were carried out as previously described (20).
597 Reaction mixtures contained 100 mM Tris-HCl (pH 7), 10 mM $MgCl_2$, 0.4 mM NADH, 4 mM,
598 50 µM $FeCl_2$, phosphoenol pyruvate (PEP), 100U/mL pig heart malate dehydrogenase(Roche),
599 2U/mL microbial PEP carboxylase (Sigma), and 10 mM 2OA. Reactions were initiated by the
600 addition of purified PP_5260 or boiled enzyme controls, and absorbance at 340 nm was
601 measured via a SpectraMax M4 plate reader (Molecular Devices, USA). Michaelis-Menten
602 behavior was formulated as previously described (46). Least-squares minimization was used to
603 derive K_m and K_{cat}. Determination of D-2HG concentration was assayed with a D-2-
604 Hydroxyglutarate (D-2HG) Assay Kit (Sigma MAK320).

605 **Acknowledgements**

This manuscript is dedicated to the memory of Cornell Professor Dr. Eugene Madsen. The authors would like to thank Morgan Price, Dr. John Hangasky, Dr. Jamie Meadows, Dr. Robert Haushalter, Dr. Bo Pang, Dr. Nick Weathersby, Mary Thompson, and Catharine Adams for their helpful discussions in preparing this manuscript. We would also like to thank the UC Berkeley SMART program for providing support for R.K to conduct summer research. This work was part of the DOE Joint BioEnergy Institute (https://www.jbei.org) supported by the U.S. Department of Energy, Office of Science, Office of Biological and Environmental Research, and protein purification and homology modelling components were part of the Agile BioFoundry (http://agilebiofoundry.org) supported by the U.S. Department of Energy, Energy Efficiency and Renewable Energy, Bioenergy Technologies Office, through contract DE-AC02-05CH11231 between Lawrence Berkeley National Laboratory and the U.S. Department of Energy. The views and opinions of the authors expressed herein do not necessarily state or reflect those of the United States Government or any agency thereof. Neither the United States Government nor any agency thereof, nor any of their employees, makes any warranty, expressed or implied, or assumes any legal liability or responsibility for the accuracy, completeness, or usefulness of any information, apparatus, product, or process disclosed, or represents that its use would not infringe privately owned rights.

Contributions

Conceptualization, M.G.T., and J.M.B.; Methodology, M.G.T., J.M.B, J.F.B., P.C.M., S.C.C., N.C.H, C.B.E, E.E.K.B, C.J.P., and A.M.D.; Investigation, M.G.T., J.M.B, W.N.S., R.A.K, J.F.B., V.T.B, P.C.M., J.W.G, C.J.P, N.C.H., F.F.T., J.H.P W.S., E.E.K.B.; Writing – Original

627 Draft, M.G.T.; Writing – Review and Editing, All authors.; Resources and supervision, P.D.A.,

628 A.P.A., A.M.D., and J.D.K.

629 **Competing Interests**

630 J.D.K. has financial interests in Amyris, Lygos, Constructive Biology, Demetrix, Napigen and

631 Maple Bio.

632 Table 1

Strain	**JBEI Part ID**	**Reference**	**Genotype**
E. coli DH10B		ThermoFisher	
E. coli S17		ATCC 47055	
E. coli BL21(DE3)		Novagen	
P. putida KT2440		ATCC 47054	
P. putida ΔPP_0158	JPUB_010967	This work	
P. putida ΔPP_2088	JPUB_013224	This work	
P. putida ΔPP_2909	JPUB_010968	This work	
P. putida ΔPP_2910	JPUB_010969	This work	
P. putida ΔPP_0158 ΔPP_2909	JPUB_010970	This work	
P. putida ΔPP_4108	JPUB_010971	This work	
P. putida ΔPP_4493	JPUB_010972	This work	
P. putida ΔPP_5260	JPUB_010973	This work	
Plasmids			
pMQ30		45	Gm, SacB
pET28		Novagen	Kan
pET21b		Novagen	Amp
pMQ30-PP_0158	JPUB_010989	This work	Gm, SacB
pMQ30-PP_2088	JPUB_013222	This work	Gm, SacB
pMQ30-PP_2909	JPUB_010991	This work	Gm, SacB
pMQ30-PP_2910	JPUB_010995	This work	Gm, SacB
pMQ30-PP_4108	JPUB_010981	This work	Gm, SacB
pMQ30-PP_4493	JPUB_010979	This work	Gm, SacB
pMQ30-PP_5260	JPUB_010977	This work	Gm, SacB

pET28-CsiD_Halo	JPUB_010987	This work	Kan
pET28-CsiD_Ecoli	JPUB_010993	This work	Kan
pET28-CsiD_Pput	JPUB_010975	This work	Kan
pET21b-PP_4108	JPUB_010983	This work	Amp
pET21b-PP_5260	JPUB_010985	This work	Amp

633

634

635

636

637 **References**

638

639 1. Nelson KE, Weinel C, Paulsen IT, Dodson RJ, Hilbert H, Martins dos Santos VAP, Fouts
640 DE, Gill SR, Pop M, Holmes M, Brinkac L, Beanan M, DeBoy RT, Daugherty S, Kolonay
641 J, Madupu R, Nelson W, White O, Peterson J, Khouri H, Fraser CM. 2002. Complete
642 genome sequence and comparative analysis of the metabolically versatile Pseudomonas
643 putida KT2440. Environ Microbiol 4:799–808.

644 2. Nikel PI, Chavarría M, Danchin A, de Lorenzo V. 2016. From dirt to industrial
645 applications: Pseudomonas putida as a Synthetic Biology chassis for hosting harsh
646 biochemical reactions. Curr Opin Chem Biol 34:20–29.

647 3. Loeschcke A, Thies S. 2015. Pseudomonas putida-a versatile host for the production of
648 natural products. Appl Microbiol Biotechnol 99:6197–6214.

649 4. Jiménez JI, Miñambres B, García JL, Díaz E. 2002. Genomic analysis of the aromatic
650 catabolic pathways from Pseudomonas putida KT2440. Environ Microbiol 4:824–841.

651 5. Ragauskas AJ, Beckham GT, Biddy MJ, Chandra R, Chen F, Davis MF, Davison BH,

652 Dixon RA, Gilna P, Keller M, Langan P, Naskar AK, Saddler JN, Tschaplinski TJ, Tuskan
653 GA, Wyman CE. 2014. Lignin valorization: improving lignin processing in the
654 biorefinery. Science 344:1246843.

655 6. Chang YF, Adams E. 1971. Induction of separate catabolic pathways for L- and D-lysine
656 in Pseudomonas putida. Biochem Biophys Res Commun 45:570–577.

657 7. Chae TU, Ko Y-S, Hwang K-S, Lee SY. 2017. Metabolic engineering of Escherichia coli
658 for the production of four-, five- and six-carbon lactams. Metab Eng 41:82–91.

659 8. Zhang J, Barajas JF, Burdu M, Wang G, Baidoo EE, Keasling JD. 2017. Application of an
660 Acyl-CoA Ligase from Streptomyces aizunensis for Lactam Biosynthesis. ACS Synth Biol
661 6:884–890.

662 9. Zhang M, Gao C, Guo X, Guo S, Kang Z, Xiao D, Yan J, Tao F, Zhang W, Dong W, Liu
663 P, Yang C, Ma C, Xu P. 2018. Increased glutarate production by blocking the glutaryl-
664 CoA dehydrogenation pathway and a catabolic pathway involving L-2-hydroxyglutarate.
665 Nat Commun 9:2114.

666 10. Kim HT, Khang TU, Baritugo K-A, Hyun SM, Kang KH, Jung SH, Song BK, Park K, Oh
667 M-K, Kim GB, Kim HU, Lee SY, Park SJ, Joo JC. 2018. Metabolic engineering of
668 Corynebacterium glutamicum for the production of glutaric acid, a C5 dicarboxylic acid
669 platform chemical. Metab Eng 51:99–109.

670 11. Revelles O, Espinosa-Urgel M, Fuhrer T, Sauer U, Ramos JL. 2005. Multiple and
671 interconnected pathways for L-lysine catabolism in Pseudomonas putida KT2440. J
672 Bacteriol 187:7500–7510.

673 12. Revelles O, Wittich R-M, Ramos JL. 2007. Identification of the initial steps in D-lysine

674 catabolism in Pseudomonas putida. J Bacteriol 189:2787–2792.

675 13. Perfetti R, Campbell RJ, Titus J, Hartline RA. 1972. Catabolism of pipecolate to glutamate
676 in Pseudomonas putida. J Biol Chem 247:4089–4095.

677 14. Wetmore KM, Price MN, Waters RJ, Lamson JS, He J, Hoover CA, Blow MJ, Bristow J,
678 Butland G, Arkin AP, Deutschbauer A. 2015. Rapid quantification of mutant fitness in
679 diverse bacteria by sequencing randomly bar-coded transposons. MBio 6:e00306-15.

680 15. Price MN, Wetmore KM, Waters RJ, Callaghan M, Ray J, Liu H, Kuehl JV, Melnyk RA,
681 Lamson JS, Suh Y, Carlson HK, Esquivel Z, Sadeeshkumar H, Chakraborty R, Zane GM,
682 Rubin BE, Wall JD, Visel A, Bristow J, Blow MJ, Deutschbauer AM. 2018. Mutant
683 phenotypes for thousands of bacterial genes of unknown function. Nature 557:503–509.

684 16. Rand JM, Pisithkul T, Clark RL, Thiede JM, Mehrer CR, Agnew DE, Campbell CE,
685 Markley AL, Price MN, Ray J, Wetmore KM, Suh Y, Arkin AP, Deutschbauer AM,
686 Amador-Noguez D, Pfleger BF. 2017. A metabolic pathway for catabolizing levulinic acid
687 in bacteria. Nat Microbiol 2:1624–1634.

688 17. Okuno E, Tsujimoto M, Nakamura M, Kido R. 1993. 2-Aminoadipate-2-oxoglutarate
689 aminotransferase isoenzymes in human liver: a plausible physiological role in lysine and
690 tryptophan metabolism. Enzyme Protein 47:136–148.

691 18. Wilding M, Peat TS, Newman J, Scott C. 2016. A β-Alanine Catabolism Pathway
692 Containing a Highly Promiscuous ω-Transaminase in the 12-Aminododecanate-Degrading
693 Pseudomonas sp. Strain AAC. Appl Environ Microbiol 82:3846–3856.

694 19. Kopchick JJ, Hartline RA. 1979. alpha-Hydroxyglutarate as an intermediate in the
695 catabolism of alpha-aminoadipate by Pseudomonas putida. J Biol Chem 254:3259–3263.

20. Witkowski A, Joshi AK, Smith S. 2002. Mechanism of the β-Ketoacyl Synthase Reaction Catalyzed by the Animal Fatty Acid Synthase†. Biochemistry 41:10877–10887.

21. Martinez S, Hausinger RP. 2016. Biochemical and Spectroscopic Characterization of the Non-Heme Fe(II)- and 2-Oxoglutarate-Dependent Ethylene-Forming Enzyme from Pseudomonas syringae pv. phaseolicola PK2. Biochemistry 55:5989–5999.

22. Martinez S, Hausinger RP. 2015. Catalytic Mechanisms of Fe(II)- and 2-Oxoglutarate-dependent Oxygenases. J Biol Chem 290:20702–20711.

23. Revelles O, Espinosa-Urgel M, Molin S, Ramos JL. 2004. The davDT operon of Pseudomonas putida, involved in lysine catabolism, is induced in response to the pathway intermediate delta-aminovaleric acid. J Bacteriol 186:3439–3446.

24. Danhauser K, Sauer SW, Haack TB, Wieland T, Staufner C, Graf E, Zschocke J, Strom TM, Traub T, Okun JG, Meitinger T, Hoffmann GF, Prokisch H, Kölker S. 2012. DHTKD1 mutations cause 2-aminoadipic and 2-oxoadipic aciduria. Am J Hum Genet 91:1082–1087.

25. REITZ M, RODWELL V. 1969. a-Hydroxyglutarate Oxidoreductase of Pseudomonas putida. J Bacteriol.

26. Wójcik A, Broclawik E, Siegbahn PEM, Borowski T. 2012. Mechanism of benzylic hydroxylation by 4-hydroxymandelate synthase. A computational study. Biochemistry 51:9570–9580.

27. Di Giuro CML, Konstantinovics C, Rinner U, Nowikow C, Leitner E, Straganz GD. 2013. Chiral hydroxylation at the mononuclear nonheme Fe(II) center of 4-(S) hydroxymandelate synthase--a structure-activity relationship analysis. PLoS ONE 8:e68932.

718 28. Lequette Y, Odberg-Ferragut C, Bohin J-P, Lacroix J-M. 2004. Identification of mdoD, an
719 mdoG paralog which encodes a twin-arginine-dependent periplasmic protein that controls
720 osmoregulated periplasmic glucan backbone structures. J Bacteriol 186:3695–3702.

721 29. Zhang L, Ren Y, Lu B, Yang C, Feng Z, Liu Z, Chen J, Ma W, Wang Y, Yu X, Wang Y,
722 Zhang W, Wang Y, Liu S, Wu F, Zhang X, Guo X, Bao Y, Jiang L, Wan J. 2016.
723 FLOURY ENDOSPERM7 encodes a regulator of starch synthesis and amyloplast
724 development essential for peripheral endosperm development in rice. J Exp Bot 67:633–
725 647.

726 30. Vijayakumar SRV, Kirchhof MG, Patten CL, Schellhorn HE. 2004. RpoS-regulated genes
727 of Escherichia coli identified by random lacZ fusion mutagenesis. J Bacteriol 186:8499–
728 8507.

729 31. Knorr S, Sinn M, Galetskiy D, Williams RM, Wang C, Müller N, Mayans O, Schleheck D,
730 Hartig JS. 2018. Widespread bacterial lysine degradation proceeding via glutarate and L-2-
731 hydroxyglutarate. Nat Commun 9:5071.

732 32. Nishijyo T, Haas D, Itoh Y. 2001. The CbrA-CbrB two-component regulatory system
733 controls the utilization of multiple carbon and nitrogen sources in Pseudomonas
734 aeruginosa. Mol Microbiol 40:917–931.

735 33. Valentini M, García-Mauriño SM, Pérez-Martínez I, Santero E, Canosa I, Lapouge K.
736 2014. Hierarchical management of carbon sources is regulated similarly by the CbrA/B
737 systems in Pseudomonas aeruginosa and Pseudomonas putida. Microbiology (Reading,
738 Engl) 160:2243–2252.

739 34. Bouffartigues E, Gicquel G, Bazire A, Bains M, Maillot O, Vieillard J, Feuilloley MGJ,

740 Orange N, Hancock REW, Dufour A, Chevalier S. 2012. Transcription of the oprF gene of
741 Pseudomonas aeruginosa is dependent mainly on the SigX sigma factor and is sucrose
742 induced. J Bacteriol 194:4301–4311.

743 35. Blanka A, Schulz S, Eckweiler D, Franke R, Bielecka A, Nicolai T, Casilag F, Düvel J,
744 Abraham W-R, Kaever V, Häussler S. 2014. Identification of the alternative sigma factor
745 SigX regulon and its implications for Pseudomonas aeruginosa pathogenicity. J Bacteriol
746 196:345–356.

747 36. Neshich IAP, Kiyota E, Arruda P. 2013. Genome-wide analysis of lysine catabolism in
748 bacteria reveals new connections with osmotic stress resistance. ISME J 7:2400–2410.

749 37. Brinkman AB, Bell SD, Lebbink RJ, de Vos WM, van der Oost J. 2002. The Sulfolobus
750 solfataricus Lrp-like protein LysM regulates lysine biosynthesis in response to lysine
751 availability. J Biol Chem 277:29537–29549.

752 38. Thaw P, Sedelnikova SE, Muranova T, Wiese S, Ayora S, Alonso JC, Brinkman AB,
753 Akerboom J, van der Oost J, Rafferty JB. 2006. Structural insight into gene transcriptional
754 regulation and effector binding by the Lrp/AsnC family. Nucleic Acids Res 34:1439–1449.

755 39. LaBauve AE, Wargo MJ. 2012. Growth and laboratory maintenance of Pseudomonas
756 aeruginosa. Curr Protoc Microbiol Chapter 6:Unit 6E.1.

757 40. Ham TS, Dmytriv Z, Plahar H, Chen J, Hillson NJ, Keasling JD. 2012. Design,
758 implementation and practice of JBEI-ICE: an open source biological part registry platform
759 and tools. Nucleic Acids Res 40:e141.

760 41. Chen J, Densmore D, Ham TS, Keasling JD, Hillson NJ. 2012. DeviceEditor visual
761 biological CAD canvas. J Biol Eng 6:1.

762 42. Hillson NJ, Rosengarten RD, Keasling JD. 2012. j5 DNA assembly design automation
763 software. ACS Synth Biol 1:14–21.

764 43. Gibson DG, Young L, Chuang R-Y, Venter JC, Hutchison CA, Smith HO. 2009.
765 Enzymatic assembly of DNA molecules up to several hundred kilobases. Nat Methods
766 6:343–345.

767 44. Engler C, Kandzia R, Marillonnet S. 2008. A one pot, one step, precision cloning method
768 with high throughput capability. PLoS ONE 3:e3647.

769 45. Shanks RMQ, Kadouri DE, MacEachran DP, O'Toole GA. 2009. New yeast
770 recombineering tools for bacteria. Plasmid 62:88–97.

771 46. Cornish-Bowden A. 2012. Fundamentals of Enzyme Kinetics, 4th ed. Wiley, John & Sons,
772 Incorporated.

Massively parallel fitness profiling reveals multiple novel enzymes in *Pseudomonas putida* lysine metabolism

Mitchell G. Thompson[1,2,3], Jacquelyn M. Blake-Hedges[1,2,4], Pablo Cruz-Morales[1,2,5], Jesus F. Barajas[2,6], Samuel C. Curran[1,2,7], Christopher B. Eiben[1,2,8], Nicholas C. Harris[3], Veronica T. Benites[1,2], Jennifer W. Gin[1,2], William A. Sharpless[1,2,3], Frederick F. Twigg[8], Will Skyrud[4], Rohith N. Krishna[1,2,4], Jose Henrique Pereira[1,9], Edward E. K. Baidoo[1,2], Christopher J. Petzold[1,2], Paul D. Adams[1,9,10], Adam P. Arkin[10,11], Adam M. Deutschbauer[3,11], Jay D. Keasling[1,2,8,10,12]

[1]Joint BioEnergy Institute, 5885 Hollis Street, Emeryville, CA 94608, USA.

[2]Biological Systems & Engineering Division, Lawrence Berkeley National Laboratory, Berkeley, CA 94720, USA.

[3]Department of Plant and Microbial Biology, University of California, Berkeley, CA 94720, USA

[4]Department of Chemistry, University of California, Berkeley, CA 94720, USA

[5]Centro de Biotecnología FEMSA, Tecnológico de Monterrey, NL, Mexico

[6]Department of Energy Agile BioFoundry, Emeryville, CA 94608, USA

[7]Comparative Biochemistry Graduate Group, University of California, Berkeley, CA 94720, USA

[8]Department of Chemical and Biomolecular Engineering, University of California, Berkeley, CA 94720, USA

[9]Molecular Biophysics and Integrated Bioimaging Division, Lawrence Berkeley National Laboratory, Berkeley, CA 94720, USA.

[10]Joint Program in Bioengineering, University of California, Berkeley/San Francisco, CA 94720, USA

[11]Environmental Genomics and Systems Biology Division, Lawrence Berkeley National Laboratory, Berkeley, CA 94720, USA.

[12]The Novo Nordisk Foundation Center for Biosustainability, Technical University of Denmark, Denmark

Supplementary Materials and Methods

HPLC analysis

HPLC analysis was performed on an Agilent Technologies 1200 series liquid chromatography instrument coupled to a refractive index detector (35°C, Agilent Technologies, Santa Clara, CA). Samples were injected onto an Aminex HPX-87H Ion Exclusion Column (300 x 7.8 mm, 60°C, Bio-Rad, Hercules, CA) and eluted isocratically with 4 mM H_2SO_4 at 600 uL/min for 20 minutes. Compounds were quantified via comparison to a calibration curve prepared with authentic standards and normalized to injection volume.

Proteomics analysis

P. putida KT2440 wild type was grown on MOPS minimal media with 10 mM of either glucose, L-lysine, D-lysine, 5AVA, 2AA, or glutarate. Cells were harvested when cultures reached an OD_{600} of 1.0 with a 1 cm pathlength. Cell lysis and protein precipitation were achieved by using a chloroform-methanol extraction as previously described (1). Thawed pellets were loosened from 14 mL falcon tubes and transferred to PCR 8-well tube strip, followed by the

addition of 80 µL of methanol, 20 µL of chloroform, and 60 µL of water, with vortexing. The samples were centrifuged at ~20,000 x g for 1 minute for phase separation. The methanol and water (top) layer was removed, then 100 µL of methanol was added and the sample was vortexed briefly. The samples were centrifuged at ~20,000 x g for 1 minute to isolate the protein pellet. The protein pellet was air-dried for 10 minutes and resuspended in 100 mM ammonium bicarbonate with 20% methanol. The protein concentration was measured using the DC Protein Assay Kit (Bio-Rad, Hercules, CA) with bovine serum albumin for the standard curve. A total of 100 µg of protein from each sample was digested with trypsin for targeted proteomic analysis. The protein was reduced by adding tris 2-(carboxyethyl) phosphine (TCEP) at a final concentration of 5 mM, alkylated by adding iodoacetamide at a final concentration of 10 mM, and digested overnight at 37 ºC with trypsin at a ratio of 1:50 (w/w) trypsin:total protein. As previously described (2), peptides were analyzed using an Agilent 1290 liquid chromatography system coupled to an Agilent 6460QQQ mass spectrometer (Agilent Technologies, Santa Clara, CA). Peptide samples (10 µg) were separated on an Ascentis Express Peptide ES-C18 column (2.7 µm particle size, 160 Å pore size, 50 mm length x 2.1 mm i.d., 60 ºC; Sigma-Aldrich, St. Louis, MO) by using a chromatographic gradient (400 µL/min flow rate) with an initial condition of 95% buffer A (99.9% water, 0.1% formic acid) and 5% buffer B (99.9% acetonitrile, 0.1% formic acid) then increasing linearly to 65% buffer A/35% buffer B over 5.5 minutes. Buffer B was then increased to 80% over 0.3 minutes and held at 80% for two minutes followed by ramping back down to 5% buffer B over 0.5 minutes where it was held for 1.5 minutes to re-equilibrate the column for the next sample. The peptides were ionized by an Agilent Jet Stream ESI source operating in positive-ion mode with the following source parameters: gas Temperature: 250 ºC, gas Flow: 13 L/min, nebulizer pressure: 35 psi, sheath gas temperature:

250 ºC, sheath gas flow: 11 L/min, nozzle voltage: 0 V, chamber voltage: 3,500 V. The data were acquired using Agilent MassHunter, version B.08.02, processed using Skyline (3) version 4.1, and peak quantification was refined with mProphet (4) in Skyline. Data are available at Panorama Public via this link: https://panoramaweb.org/massive_fitness_profiling_Pseudomonas_putida.url. All pairwise combinations of spectral counts from carbon sources for each protein were compared via Student's t-test followed by a Bonferroni correction.

Detection of metabolites

Sampling of intracellular metabolites was conducted as described previously (5). Multiple methods were used to detect compounds in this work. Method (1) HILIC-HRMS analysis was performed using an Agilent Technologies 6510 Accurate-Mass Q-TOF LC-MS instrument using positive mode and an Atlantis HILIC Silica 5 µm column (150 x 4.6 mm) with a linear of 95 to 50% acetonitrile (v/v) over 8 minutes in water with 40 mM ammonium formate, pH 4.5, at a flow rate of 1 mL $minute^{-1}$. Method (2) HILIC-HRMS analysis was performed using an Agilent Technologies 6510 Accurate-Mass Q-TOF LC-MS instrument using negative mode and an Atlantis HILIC Silica 5 µm column (150 x 4.6 mm) with an isocratic mobile phase (80% acetonitrile (v/v) with 40 mM ammonium formate, pH 4.5) for 20 minute at a flow rate of 1 mL $minute^{-1}$. Method (3) is described in George et al (5). Briefly, samples were separated via a SeQuantZIC-pHILIC guard column (20-mm length, 2.1-mm internal diameter, and 5-µm particle size; from EMD Millipore, Billerica, MA, USA), then with a short SeQuantZIC-pHILIC column (50-mm length, 2.1-mm internal diameter, and 5-µm particle size) followed by a long SeQuantZIC-pHILIC column (150-mm length, 2.1-mm internal diameter, and 5-µm particle size) using an Agilent Technologies 1200 Series Rapid Resolution HPLC system (Agilent

Technologies, Santa Clara, CA, USA). The mobile phase was composed of 10 mM ammonium carbonate and 118.4 mM ammonium hydroxide in acetonitrile/water (60.2:39.8, v/v). Metabolites were eluted isocratically via a flow rate of 0.18 mL/min from 0 to 5.4 minutes, which was increased to 0.27 mL/min from 5.4 to 5.7 minutes, and held at this flow rate for an additional 5.4 minutes. The HPLC system was coupled to an Agilent Technologies 6210 TOF-MS system in negative mode. Determination of D-2HG concentration was assayed with a D-2-Hydroxyglutarate (D2HG) Assay Kit (Sigma MAK320).

Phylogenomic analyses

Amino acid sequences of CsiD homologs were downloaded from the pFAM database and aligned with MAFFT-linsi (13). Phylogenetic trees of CsiD alignments were constructed with FastTree 2, and trees were visualized on iTOL (14, 15).

Representative DUF1338 sequences were obtained from pFAM (https://pfam.xfam.org/family/PF07063#tabview=tab3). All genomes analyzed were downloaded from the NCBI FTP site and annotated using RAST (16). Amino acid sequences of DUF1338 proteins from these genomes were retrieved using BlastP with a bit score cutoff of 150 and an E-value of 0.000001. All sequences alignments were performed using Muscle v3.8 (17) and the alignments were manually curated using Jalview V2 (18).

For the phylogenetic reconstructions, the best amino acid substitution model was selected using ModelFinder implemented on IQ-tree (19) the phylogenies were obtained using IQ-tree v 1.6.7 (20), with 10,000 bootstrap replicates. The final trees were visualized and annotated using FigTree v1.4.3 (http://tree.bio.ed.ac.uk/software/figtree/). Genome neighborhoods of DUF1338 were obtained using CORASON-BGC (21) and manually colored and annotated.

Statistical analyses and data presentation

All numerical data were analyzed using custom Python scripts. All graphs were visualized using either Seaborn or Matplotlib. Calculation of 95% confidence intervals, standard deviations, and T-test statistics were conducted via the Scipy library. Bonferroni corrections were calculated using the MNE python library (22).

Bibliography

1. González Fernández-Niño SM, Smith-Moritz AM, Chan LJG, Adams PD, Heazlewood JL, Petzold CJ. 2015. Standard flow liquid chromatography for shotgun proteomics in bioenergy research. Front Bioeng Biotechnol 3:44.

2. Batth TS, Singh P, Ramakrishnan VR, Sousa MML, Chan LJG, Tran HM, Luning EG, Pan EHY, Vuu KM, Keasling JD, Adams PD, Petzold CJ. 2014. A targeted proteomics toolkit for high-throughput absolute quantification of Escherichia coli proteins. Metab Eng 26:48–56.

3. MacLean B, Tomazela DM, Shulman N, Chambers M, Finney GL, Frewen B, Kern R, Tabb DL, Liebler DC, MacCoss MJ. 2010. Skyline: an open source document editor for creating and analyzing targeted proteomics experiments. Bioinformatics 26:966–968.

4. Reiter L, Rinner O, Picotti P, Hüttenhain R, Beck M, Brusniak M-Y, Hengartner MO, Aebersold R. 2011. mProphet: automated data processing and statistical validation for large-scale SRM experiments. Nat Methods 8:430–435.

5. George KW, Thompson MG, Kim J, Baidoo EEK, Wang G, Benites VT, Petzold CJ, Chan LJG, Yilmaz S, Turhanen P, Adams PD, Keasling JD, Lee TS. 2018. Integrated analysis of isopentenyl pyrophosphate (IPP) toxicity in isoprenoid-producing Escherichia coli. Metab Eng 47:60–72.

6. Zhang Y. 2008. I-TASSER server for protein 3D structure prediction. BMC Bioinformatics 9:40.

7. Roy A, Kucukural A, Zhang Y. 2010. I-TASSER: a unified platform for automated protein

structure and function prediction. Nat Protoc 5:725–738.

8. Yang J, Yan R, Roy A, Xu D, Poisson J, Zhang Y. 2015. The I-TASSER Suite: protein structure and function prediction. Nat Methods 12:7–8.

9. Pettersen EF, Goddard TD, Huang CC, Couch GS, Greenblatt DM, Meng EC, Ferrin TE. 2004. UCSF Chimera—a visualization system for exploratory research and analysis. J Comput Chem 25:1605–1612.

10. Adams PD, Afonine PV, Bunkóczi G, Chen VB, Davis IW, Echols N, Headd JJ, Hung L-W, Kapral GJ, Grosse-Kunstleve RW, McCoy AJ, Moriarty NW, Oeffner R, Read RJ, Richardson DC, Richardson JS, Terwilliger TC, Zwart PH. 2010. PHENIX: a comprehensive Python-based system for macromolecular structure solution. Acta Crystallogr D Biol Crystallogr 66:213–221.

11. Grosdidier A, Zoete V, Michielin O. 2011. SwissDock, a protein-small molecule docking web service based on EADock DSS. Nucleic Acids Res 39:W270-7.

12. Grosdidier A, Zoete V, Michielin O. 2011. Fast docking using the CHARMM force field with EADock DSS. J Comput Chem 32:2149–2159.

13. Katoh K, Standley DM. 2013. MAFFT multiple sequence alignment software version 7: improvements in performance and usability. Mol Biol Evol 30:772–780.

14. Price MN, Dehal PS, Arkin AP. 2010. FastTree 2--approximately maximum-likelihood trees for large alignments. PLoS ONE 5:e9490.

15. Letunic I, Bork P. 2016. Interactive tree of life (iTOL) v3: an online tool for the display and annotation of phylogenetic and other trees. Nucleic Acids Res 44:W242-5.

16. Aziz RK, Bartels D, Best AA, DeJongh M, Disz T, Edwards RA, Formsma K, Gerdes S, Glass EM, Kubal M, Meyer F, Olsen GJ, Olson R, Osterman AL, Overbeek RA, McNeil LK, Paarmann D, Paczian T, Parrello B, Pusch GD, Zagnitko O. 2008. The RAST Server: rapid annotations using subsystems technology. BMC Genomics 9:75.

17. Edgar RC. 2004. MUSCLE: multiple sequence alignment with high accuracy and high

throughput. Nucleic Acids Res 32:1792–1797.

18. Waterhouse AM, Procter JB, Martin DMA, Clamp M, Barton GJ. 2009. Jalview Version 2--a multiple sequence alignment editor and analysis workbench. Bioinformatics 25:1189–1191.

19. Kalyaanamoorthy S, Minh BQ, Wong TKF, von Haeseler A, Jermiin LS. 2017. ModelFinder: fast model selection for accurate phylogenetic estimates. Nat Methods 14:587–589.

20. Nguyen L-T, Schmidt HA, von Haeseler A, Minh BQ. 2015. IQ-TREE: a fast and effective stochastic algorithm for estimating maximum-likelihood phylogenies. Mol Biol Evol 32:268–274.

21. Cruz-Morales P, Ramos-Aboites HE, Licona-Cassani C, Selem-Mójica N, Mejía-Ponce PM, Souza-Saldívar V, Barona-Gómez F. 2017. Actinobacteria phylogenomics, selective isolation from an iron oligotrophic environment and siderophore functional characterization, unveil new desferrioxamine traits. FEMS Microbiol Ecol 93.

22. Gramfort A, Luessi M, Larson E, Engemann DA, Strohmeier D, Brodbeck C, Parkkonen L, Hämäläinen MS. 2014. MNE software for processing MEG and EEG data. Neuroimage 86:446–460.

A

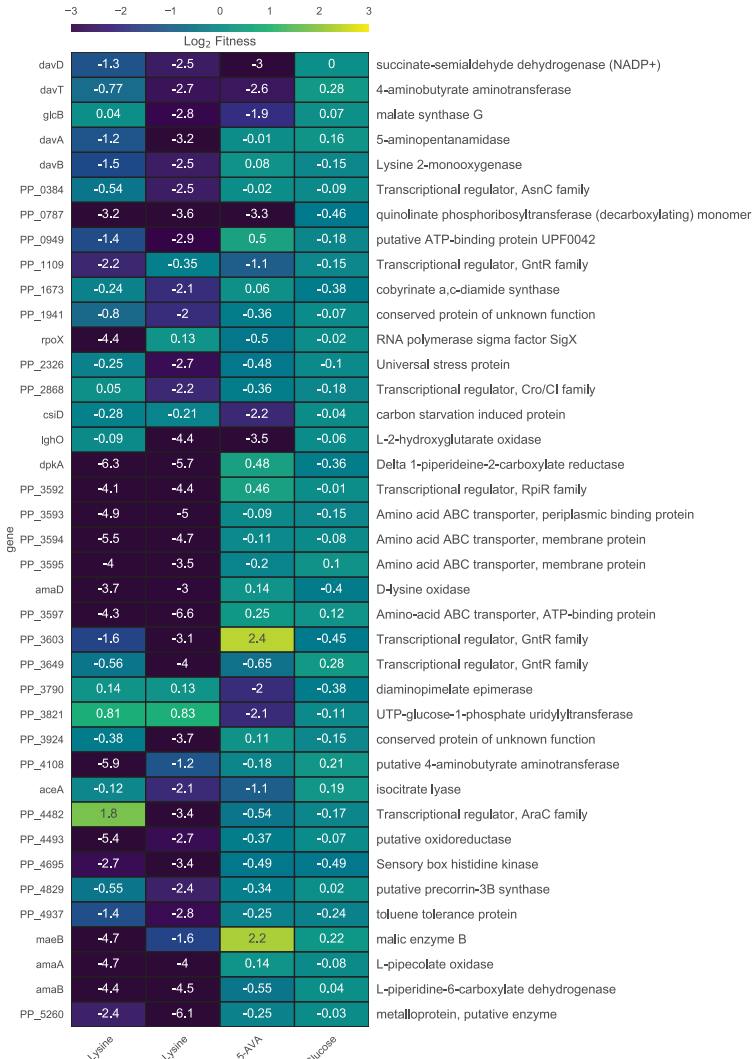

gene	D-Lysine	L-Lysine	5-AVA	Glucose	
davD	-1.3	-2.5	-3	0	succinate-semialdehyde dehydrogenase (NADP+)
davT	-0.77	-2.7	-2.6	0.28	4-aminobutyrate aminotransferase
glcB	0.04	-2.8	-1.9	0.07	malate synthase G
davA	-1.2	-3.2	-0.01	0.16	5-aminopentanamidase
davB	-1.5	-2.5	0.08	-0.15	Lysine 2-monooxygenase
PP_0384	-0.54	-2.5	-0.02	-0.09	Transcriptional regulator, AsnC family
PP_0787	-3.2	-3.6	-3.3	-0.46	quinolinate phosphoribosyltransferase (decarboxylating) monomer
PP_0949	-1.4	-2.9	0.5	-0.18	putative ATP-binding protein UPF0042
PP_1109	-2.2	-0.35	-1.1	-0.15	Transcriptional regulator, GntR family
PP_1673	-0.24	-2.1	0.06	-0.38	cobyrinate a,c-diamide synthase
PP_1941	-0.8	-2	-0.36	-0.07	conserved protein of unknown function
rpoX	-4.4	0.13	-0.5	-0.02	RNA polymerase sigma factor SigX
PP_2326	-0.25	-2.7	-0.48	-0.1	Universal stress protein
PP_2868	0.05	-2.2	-0.36	-0.18	Transcriptional regulator, Cro/CI family
csiD	-0.28	-0.21	-2.2	-0.04	carbon starvation induced protein
lghO	-0.09	-4.4	-3.5	-0.06	L-2-hydroxyglutarate oxidase
dpkA	-6.3	-5.7	0.48	-0.36	Delta 1-piperideine-2-carboxylate reductase
PP_3592	-4.1	-4.4	0.46	-0.01	Transcriptional regulator, RpiR family
PP_3593	-4.9	-5	-0.09	-0.15	Amino acid ABC transporter, periplasmic binding protein
PP_3594	-5.5	-4.7	-0.11	-0.08	Amino acid ABC transporter, membrane protein
PP_3595	-4	-3.5	-0.2	0.1	Amino acid ABC transporter, membrane protein
amaD	-3.7	-3	0.14	-0.4	D-lysine oxidase
PP_3597	-4.3	-6.6	0.25	0.12	Amino-acid ABC transporter, ATP-binding protein
PP_3603	-1.6	-3.1	2.4	-0.45	Transcriptional regulator, GntR family
PP_3649	-0.56	-4	-0.65	0.28	Transcriptional regulator, GntR family
PP_3790	0.14	0.13	-2	-0.38	diaminopimelate epimerase
PP_3821	0.81	0.83	-2.1	-0.11	UTP-glucose-1-phosphate uridylyltransferase
PP_3924	-0.38	-3.7	0.11	-0.15	conserved protein of unknown function
PP_4108	-5.9	-1.2	-0.18	0.21	putative 4-aminobutyrate aminotransferase
aceA	-0.12	-2.1	-1.1	0.19	isocitrate lyase
PP_4482	1.8	-3.4	-0.54	-0.17	Transcriptional regulator, AraC family
PP_4493	-5.4	-2.7	-0.37	-0.07	putative oxidoreductase
PP_4695	-2.7	-3.4	-0.49	-0.49	Sensory box histidine kinase
PP_4829	-0.55	-2.4	-0.34	0.02	putative precorrin-3B synthase
PP_4937	-1.4	-2.8	-0.25	-0.24	toluene tolerance protein
maeB	-4.7	-1.6	2.2	0.22	malic enzyme B
amaA	-4.7	-4	0.14	-0.08	L-pipecolate oxidase
amaB	-4.4	-4.5	-0.55	0.04	L-piperidine-6-carboxylate dehydrogenase
PP_5260	-2.4	-6.1	-0.25	-0.03	metalloprotein, putative enzyme

B

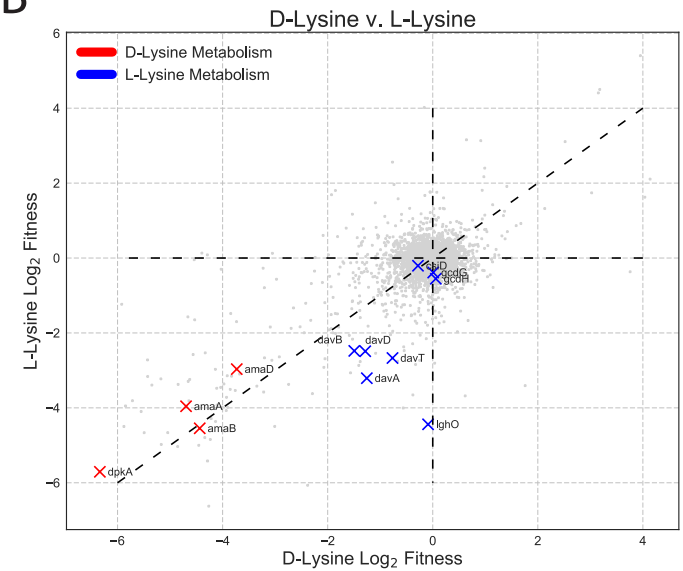

C

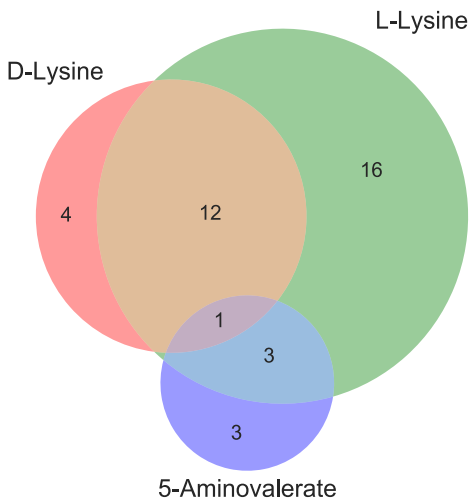

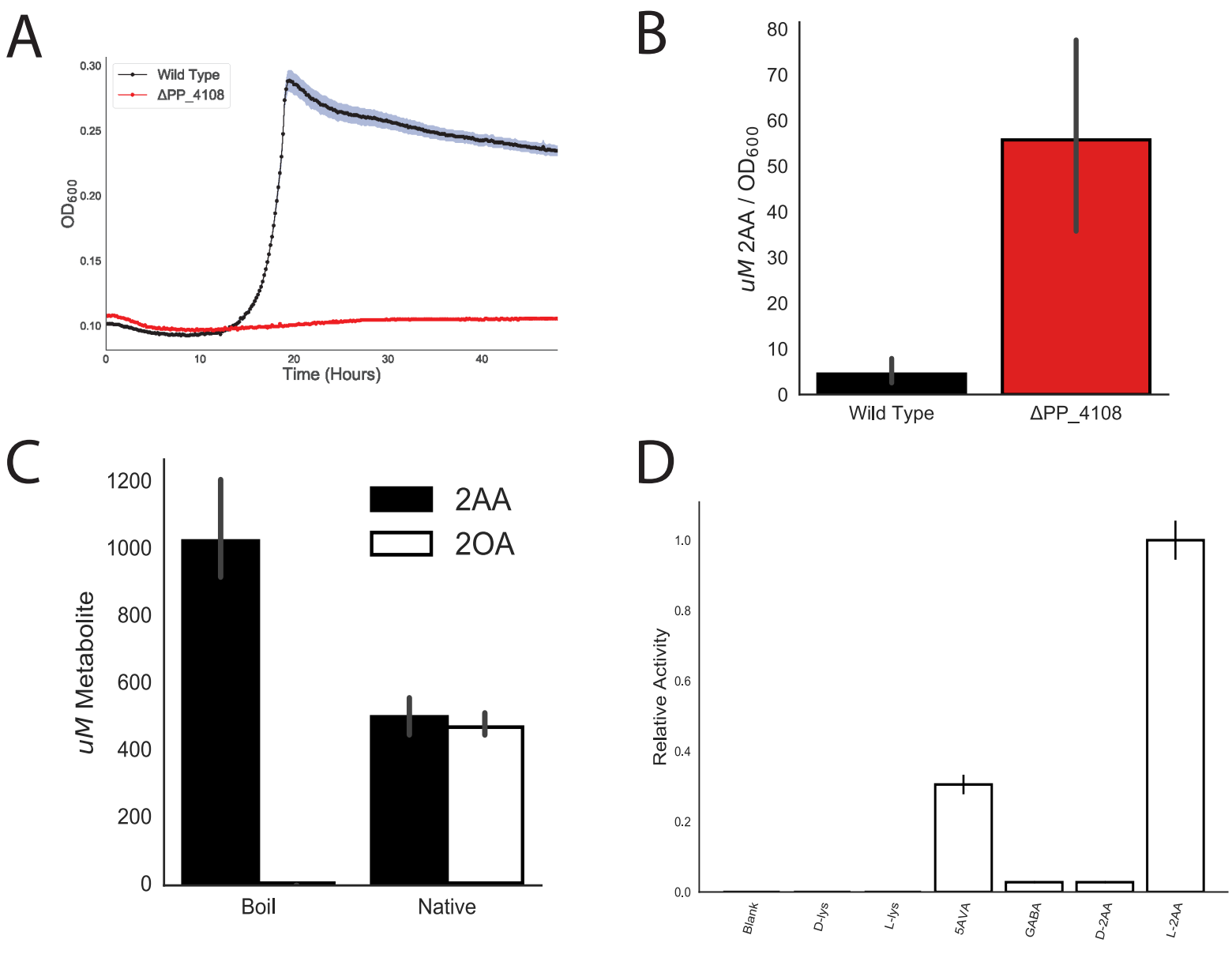
A
Wild Type
ΔPP_4108
OD600
Time (Hours)
B
uM 2AA / OD600
Wild Type
ΔPP_4108
C
2AA
2OA
uM Metabolite
Boil
Native
D
Relative Activity
Blank
D-lys
L-lys
5AVA
GABA
D-2AA
L-2AA

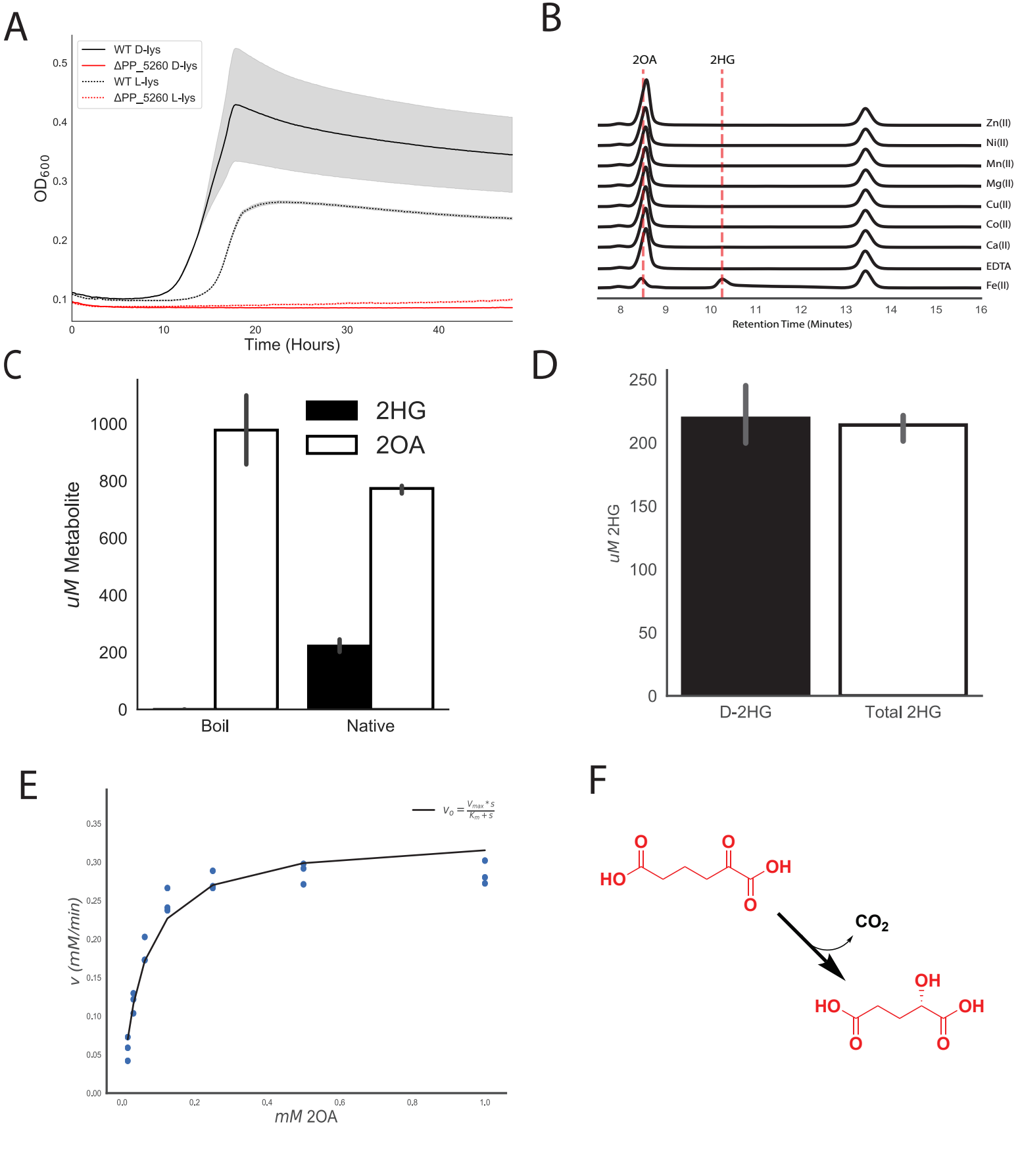
A
WT D-lys
ΔPP_5260 D-lys
WT L-lys
ΔPP_5260 L-lys
OD600
Time (Hours)
B
2OA
2HG
Zn(II)
Ni(II)
Mn(II)
Mg(II)
Cu(II)
Co(II)
Ca(II)
EDTA
Fe(II)
Retention Time (Minutes)
C
2HG
2OA
uM Metabolite
Boil
Native
D
uM 2HG
D-2HG
Total 2HG
E
mM 2OA
v (mM/min)
F
CO2

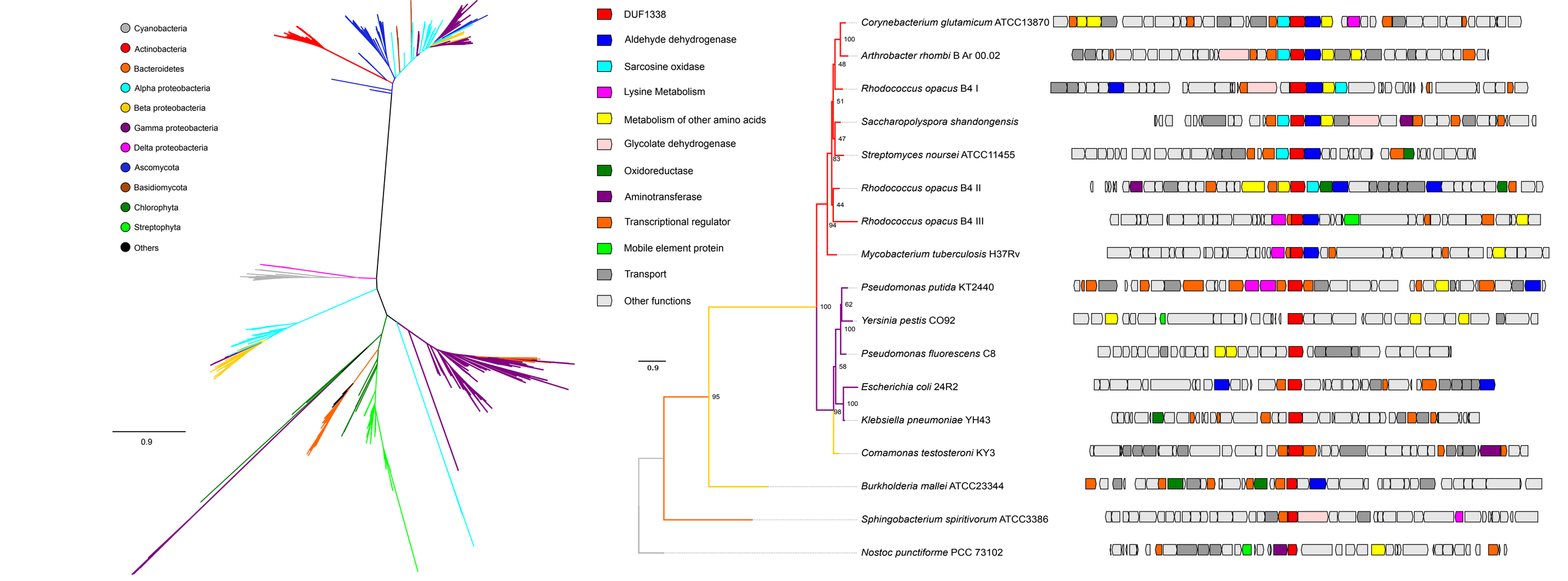
Cyanobacteria
Actinobacteria
Bacteroidetes
Alpha proteobacteria
Beta proteobacteria
Gamma proteobacteria
Delta proteobacteria
Ascomycota
Basidiomycota
Chlorophyta
Streptophyta
Others
0.9
DUF1338
Aldehyde dehydrogenase
Sarcosine oxidase
Lysine Metabolism
Metabolism of other amino acids
Glycolate dehydrogenase
Oxidoreductase
Aminotransferase
Transcriptional regulator
Mobile element protein
Transport
Other functions
0.9
Corynebacterium glutamicum ATCC13870
Arthrobacter rhombi B Ar 00.02
Rhodococcus opacus B4 I
Saccharopolyspora shandongensis
Streptomyces noursei ATCC11455
Rhodococcus opacus B4 II
Rhodococcus opacus B4 III
Mycobacterium tuberculosis H37Rv
Pseudomonas putida KT2440
Yersinia pestis CO92
Pseudomonas fluorescens C8
Escherichia coli 24R2
Klebsiella pneumoniae YH43
Comamonas testosteroni KY3
Burkholderia mallei ATCC23344
Sphingobacterium spiritivorum ATCC3386
Nostoc punctiforme PCC 73102
100
48
51
47
83
44
94
100
62
100
58
100
98
95

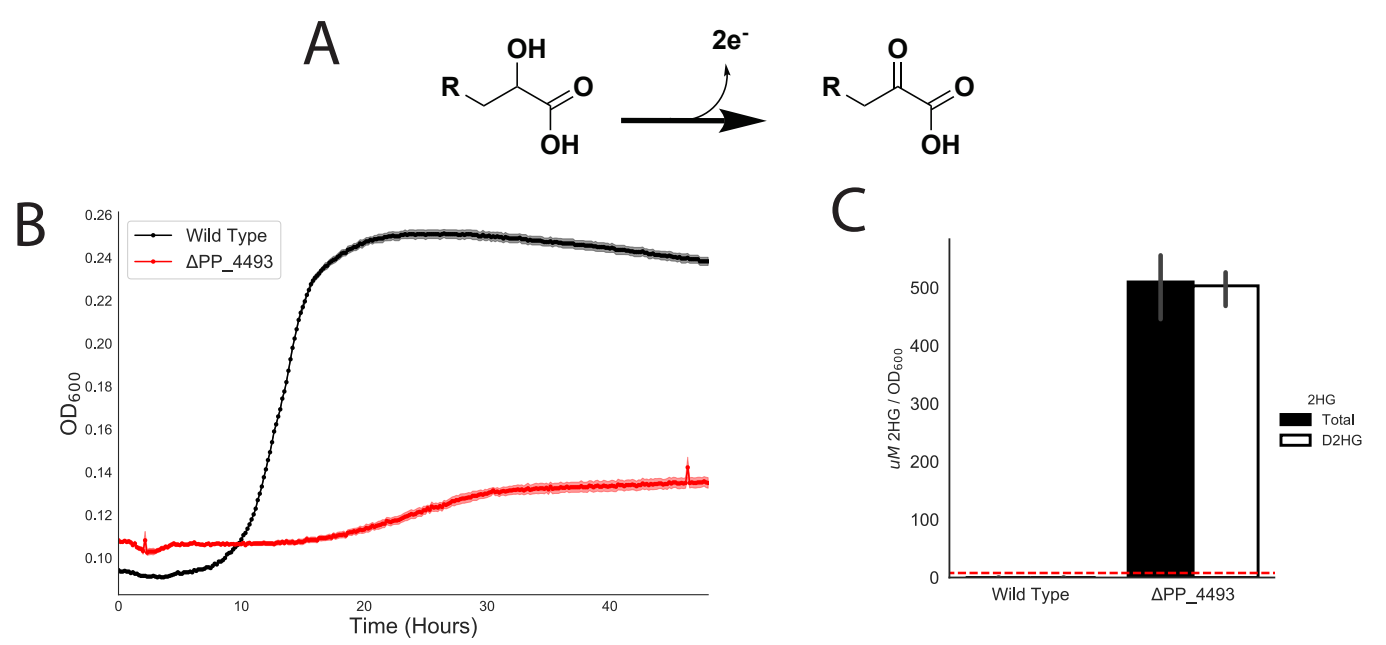
A
OH
R
O
OH
2e-
O
R
O
OH
B
Wild Type
ΔPP_4493
OD600
0.26
0.24
0.22
0.20
0.18
0.16
0.14
0.12
0.10
0
10
20
30
40
Time (Hours)
C
uM 2HG / OD600
500
400
300
200
100
0
Wild Type
ΔPP_4493
2HG
Total
D2HG

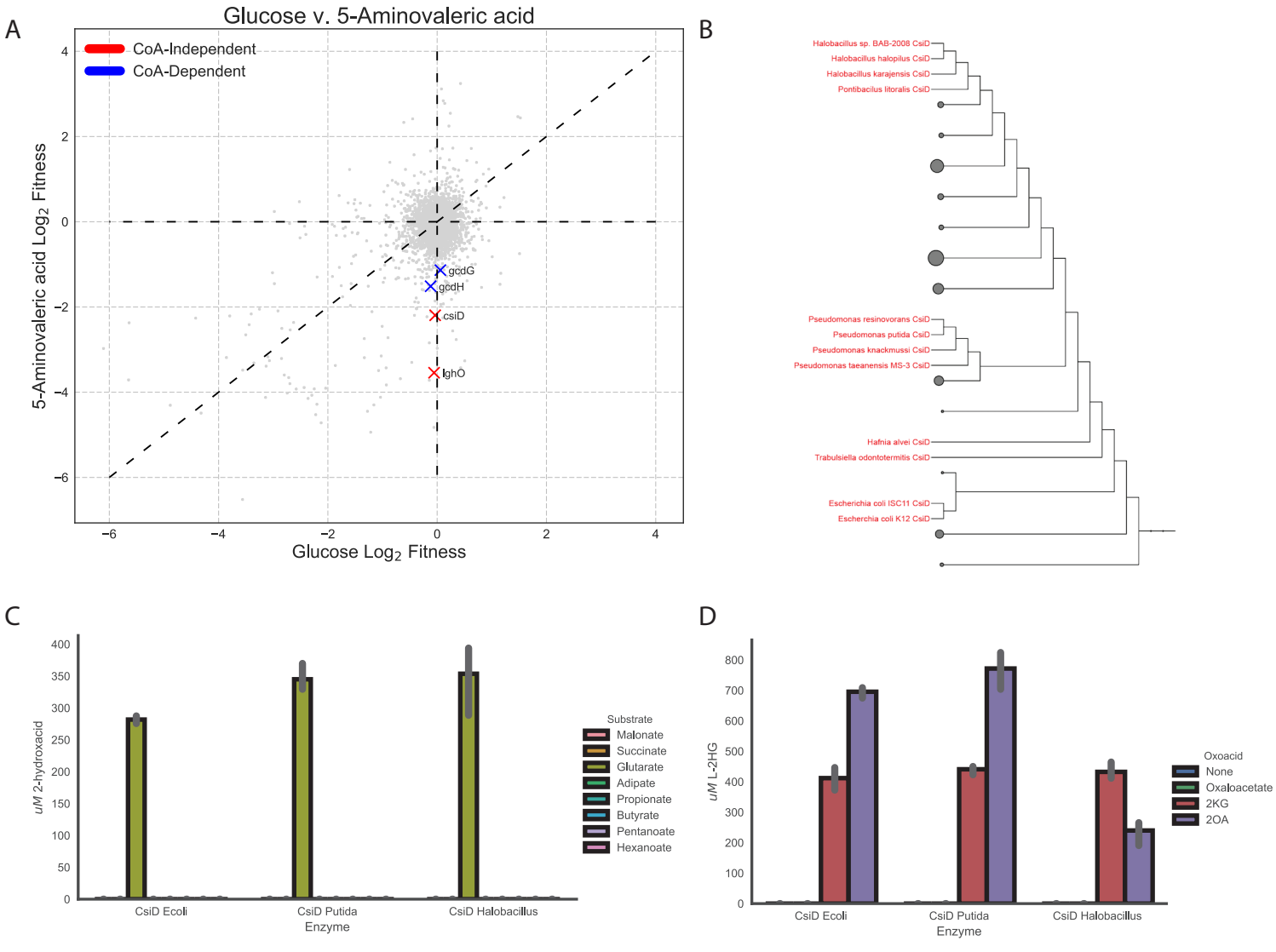
A
Glucose v. 5-Aminovaleric acid
CoA-Independent
CoA-Dependent
gcdG
gcdH
csiD
lghO
5-Aminovaleric acid Log2 Fitness
Glucose Log2 Fitness
B
Halobacillus sp. BAB-2008 CsiD
Halobacillus halopilus CsiD
Halobacillus karajensis CsiD
Pontibacillus litoralis CsiD
Pseudomonas resinovorans CsiD
Pseudomonas putida CsiD
Pseudomonas knackmussi CsiD
Pseudomonas taeanensis MS-3 CsiD
Hafnia alvei CsiD
Trabulsiella odontotermitis CsiD
Escherichia coli ISC11 CsiD
Escherchia coli K12 CsiD
C
uM 2-hydroxacid
CsiD Ecoli
CsiD Putida
CsiD Halobacillus
Enzyme
Substrate
Malonate
Succinate
Glutarate
Adipate
Propionate
Butyrate
Pentanoate
Hexanoate
D
uM L-2HG
CsiD Ecoli
CsiD Putida
CsiD Halobacillus
Enzyme
Oxoacid
None
Oxaloacetate
2KG
2OA

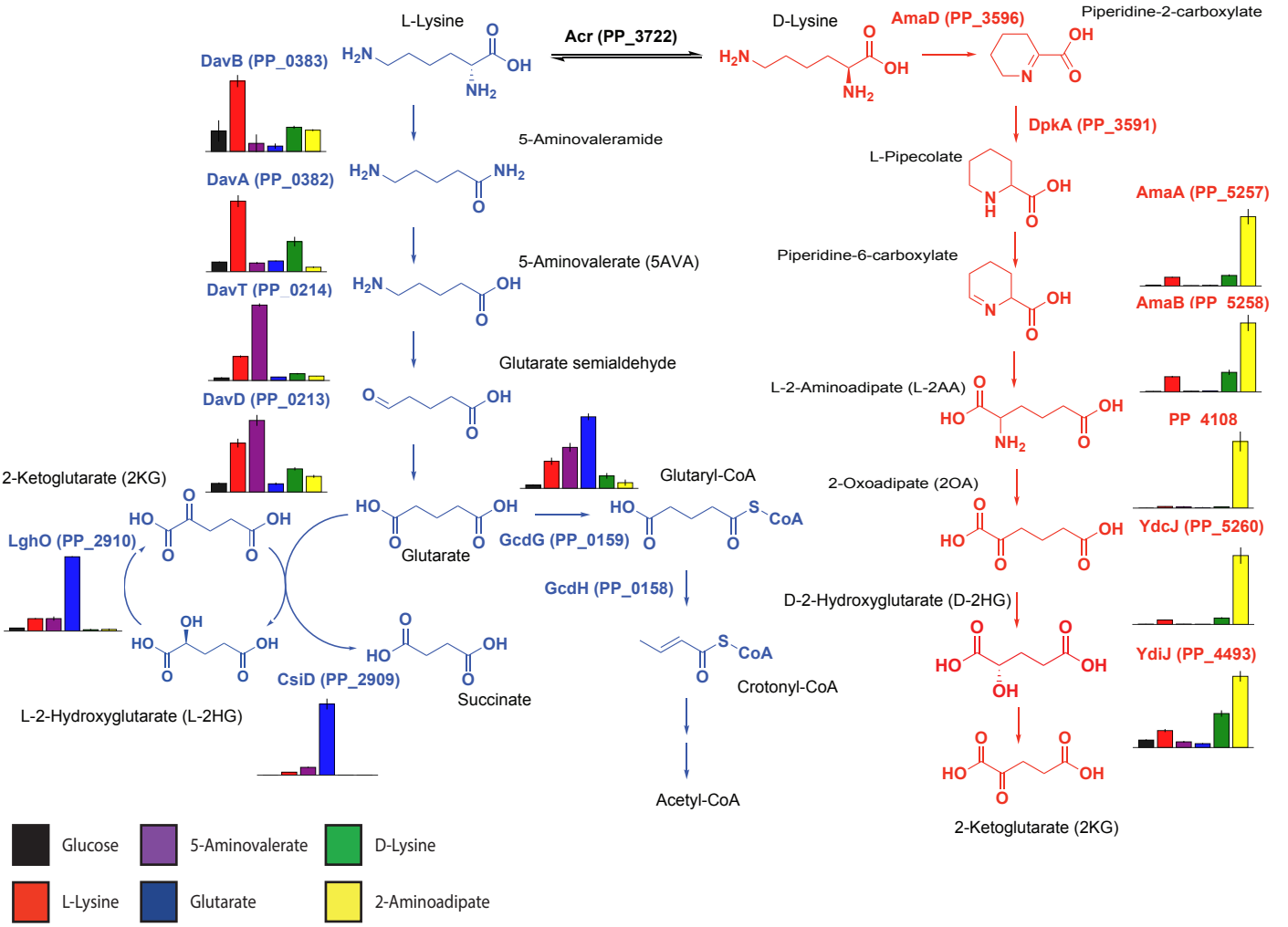
L-Lysine
Acr (PP_3722)
D-Lysine
AmaD (PP_3596)
Piperidine-2-carboxylate
DavB (PP_0383)
5-Aminovaleramide
DpkA (PP_3591)
L-Pipecolate
DavA (PP_0382)
AmaA (PP_5257)
5-Aminovalerate (5AVA)
Piperidine-6-carboxylate
DavT (PP_0214)
AmaB (PP_5258)
Glutarate semialdehyde
L-2-Aminoadipate (L-2AA)
DavD (PP_0213)
PP_4108
2-Ketoglutarate (2KG)
Glutaryl-CoA
2-Oxoadipate (2OA)
LghO (PP_2910)
Glutarate
GcdG (PP_0159)
YdcJ (PP_5260)
GcdH (PP_0158)
D-2-Hydroxyglutarate (D-2HG)
CsiD (PP_2909)
Succinate
YdiJ (PP_4493)
Crotonyl-CoA
L-2-Hydroxyglutarate (L-2HG)
Acetyl-CoA
2-Ketoglutarate (2KG)
Glucose
5-Aminovalerate
D-Lysine
L-Lysine
Glutarate
2-Aminoadipate

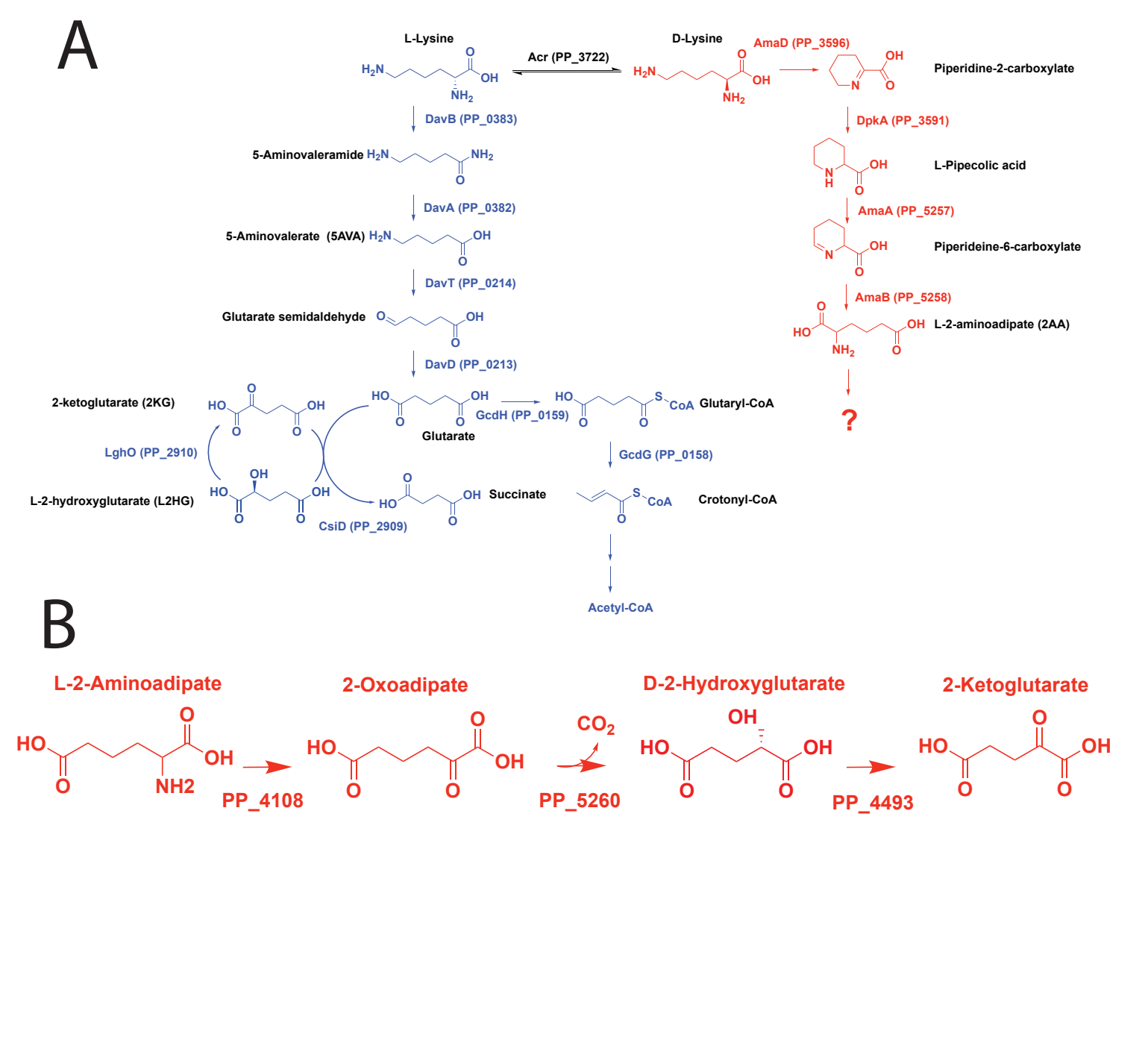
A
L-Lysine
Acr (PP_3722)
D-Lysine
AmaD (PP_3596)
Piperidine-2-carboxylate
DavB (PP_0383)
DpkA (PP_3591)
5-Aminovaleramide
L-Pipecolic acid
DavA (PP_0382)
AmaA (PP_5257)
5-Aminovalerate (5AVA)
Piperideine-6-carboxylate
DavT (PP_0214)
AmaB (PP_5258)
Glutarate semidaldehyde
L-2-aminoadipate (2AA)
DavD (PP_0213)
?
2-ketoglutarate (2KG)
GcdH (PP_0159)
Glutaryl-CoA
Glutarate
LghO (PP_2910)
GcdG (PP_0158)
L-2-hydroxyglutarate (L2HG)
Succinate
Crotonyl-CoA
CsiD (PP_2909)
Acetyl-CoA
B
L-2-Aminoadipate
2-Oxoadipate
D-2-Hydroxyglutarate
2-Ketoglutarate
PP_4108
PP_5260
PP_4493

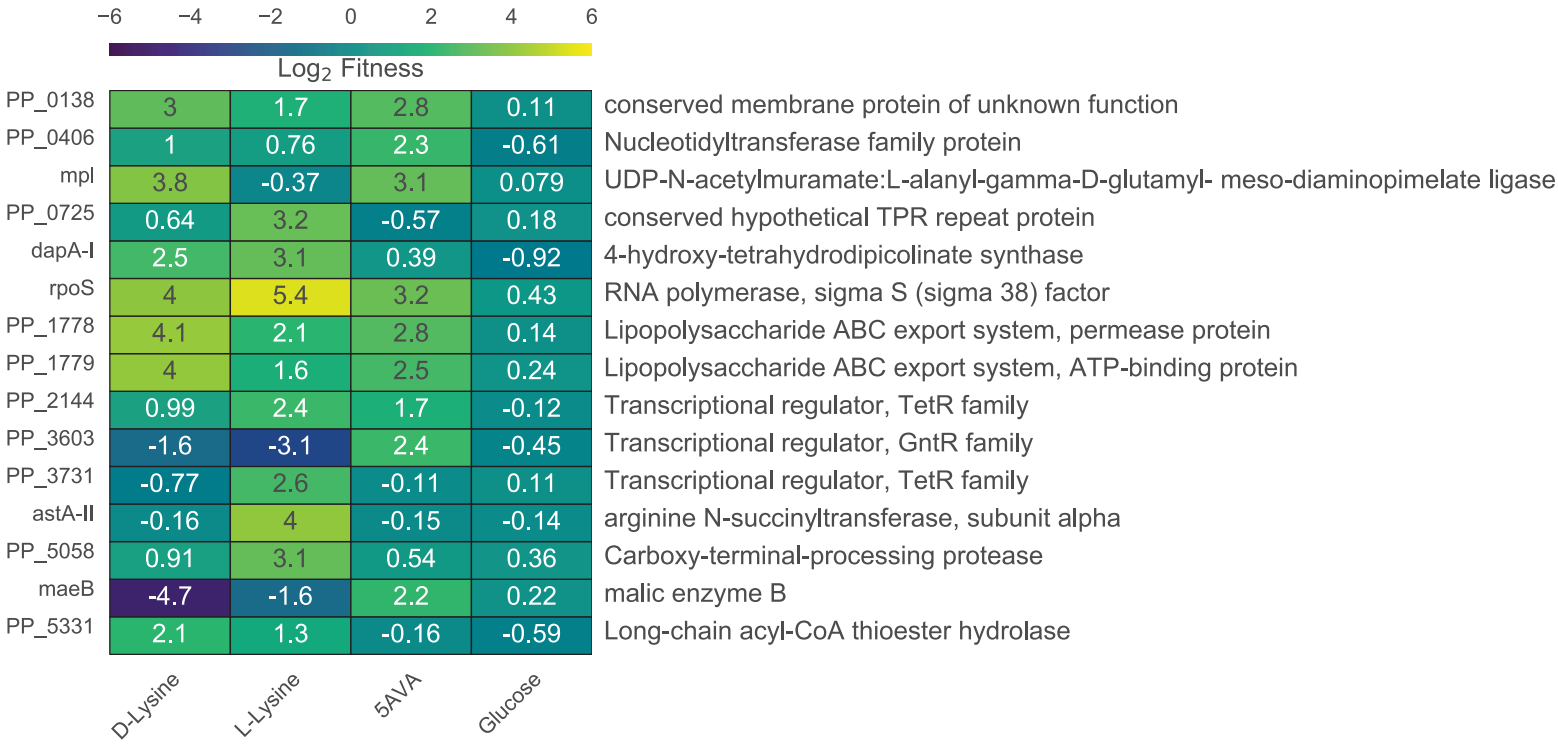

Figure S2: Results of RB-TnSeq screen. A) Genes that showed great than 2 log2 fitness on either D-lysine, L-lysine, or 5AVA but showed no less than 0.5 log2 fitness defect when grown on glucose.

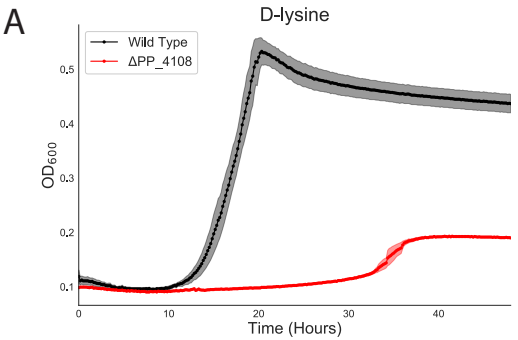
A
D-lysine
Wild Type
ΔPP_4108
OD600
Time (Hours)

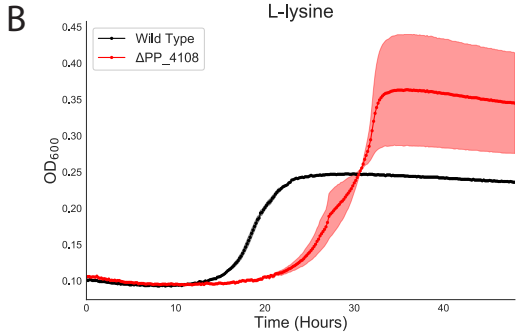
B
L-lysine
Wild Type
ΔPP_4108
OD600
Time (Hours)

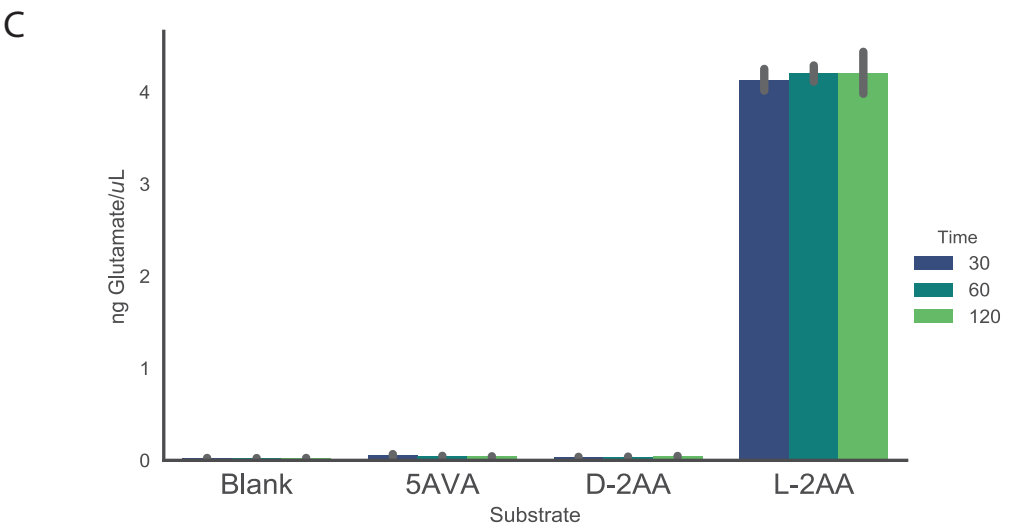
C
ng Glutamate/uL
Blank
5AVA
D-2AA
L-2AA
Substrate
Time
30
60
120

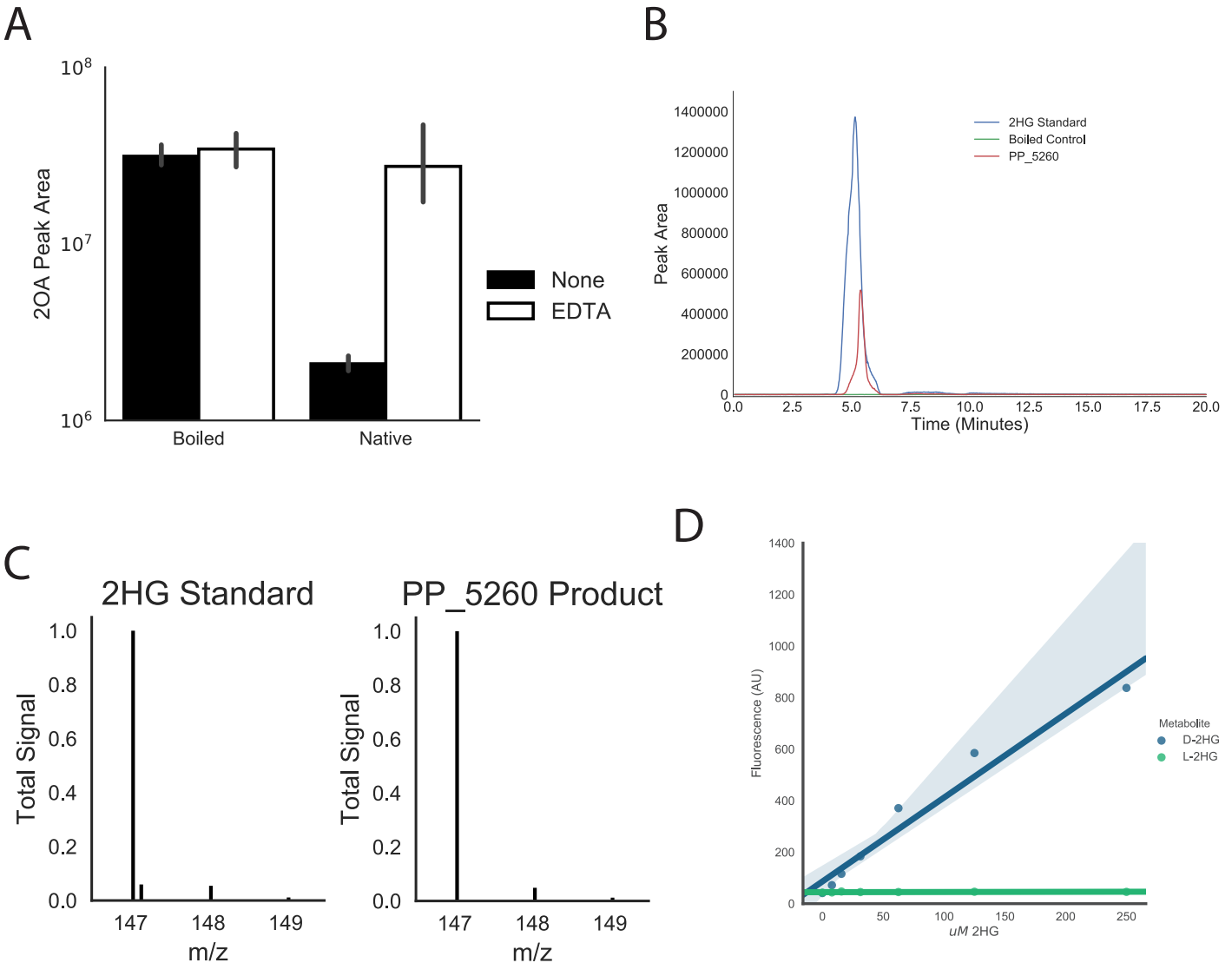
A
10^8
10^7
10^6
2OA Peak Area
None
EDTA
Boiled
Native
B
1400000
1200000
1000000
800000
600000
400000
200000
0
Peak Area
2HG Standard
Boiled Control
PP_5260
0.0
2.5
5.0
7.5
10.0
12.5
15.0
17.5
20.0
Time (Minutes)
C
2HG Standard
PP_5260 Product
Total Signal
1.0
0.8
0.6
0.4
0.2
0.0
147
148
149
m/z
D
1400
1200
1000
800
600
400
200
0
Fluorescence (AU)
0
50
100
150
200
250
uM 2HG
Metabolite
D-2HG
L-2HG

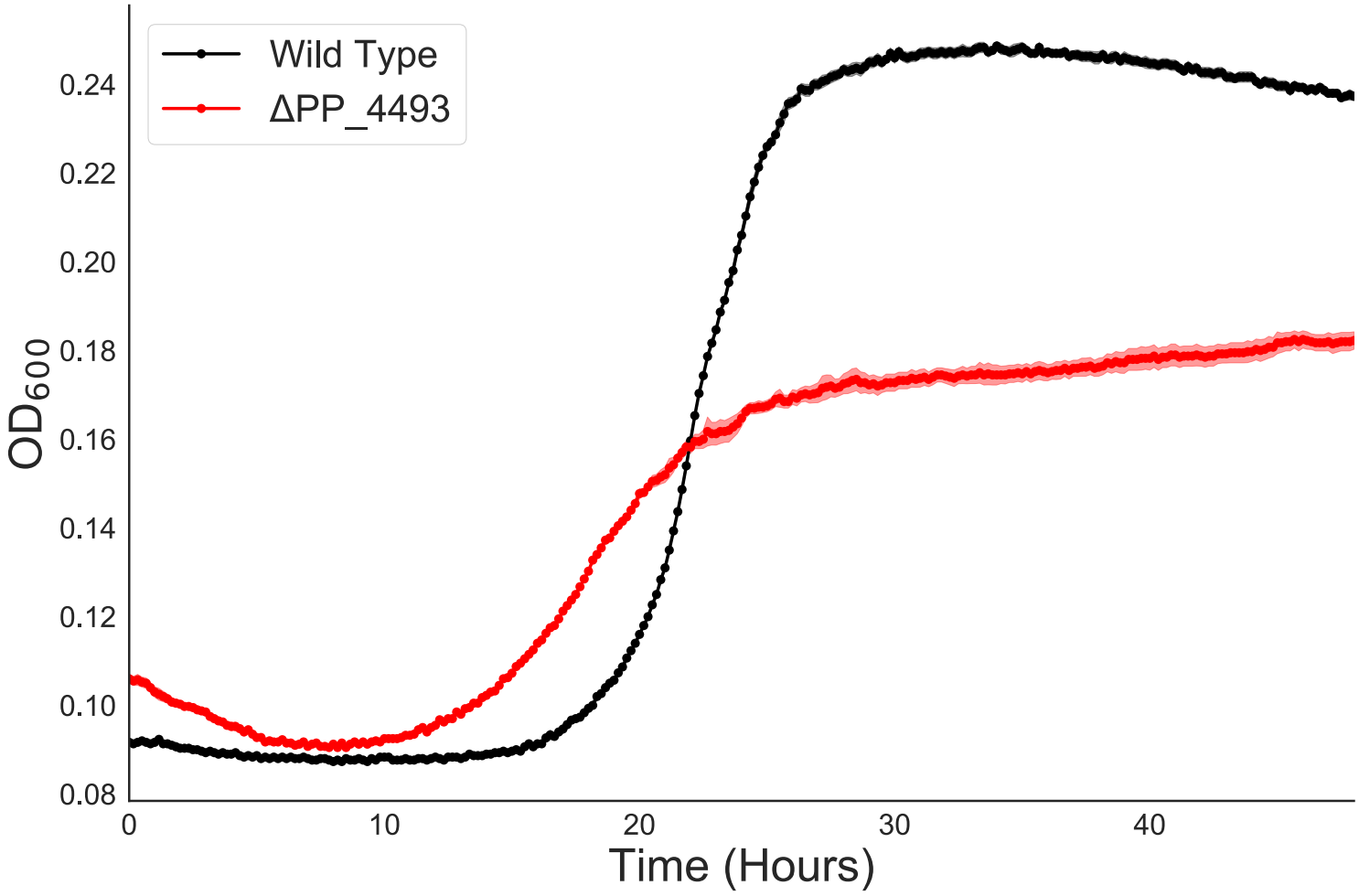
Wild Type
ΔPP_4493
0.24
0.22
0.20
0.18
0.16
0.14
0.12
0.10
0.08
OD600
0
10
20
30
40
Time (Hours)

A

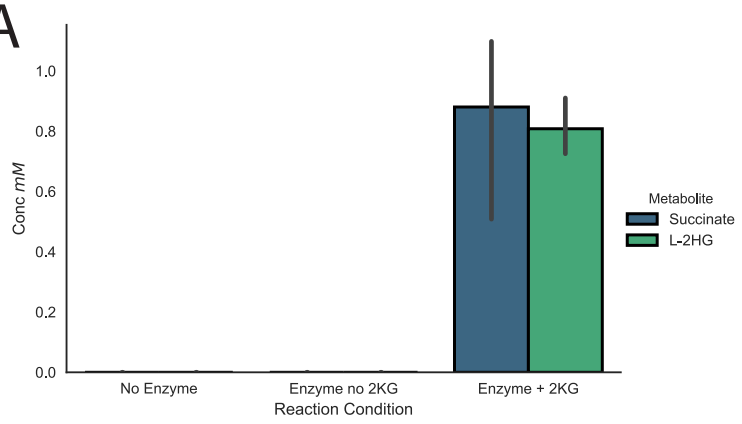

B

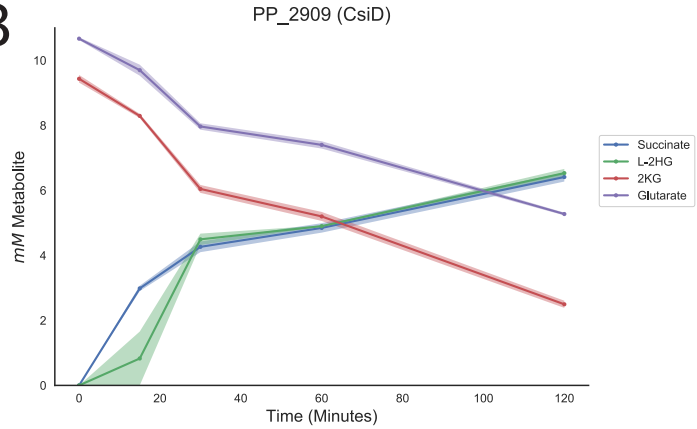

C

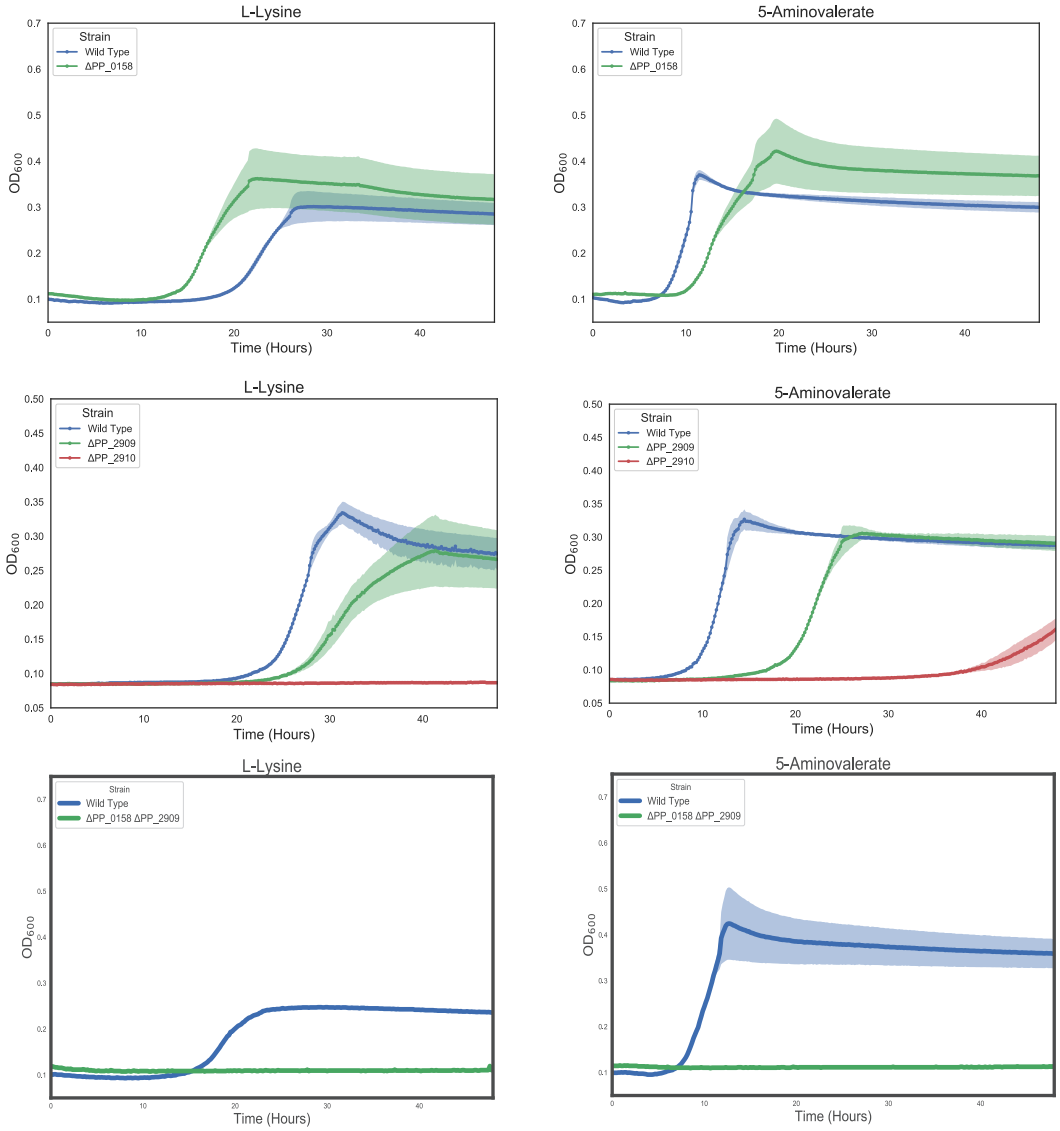

A

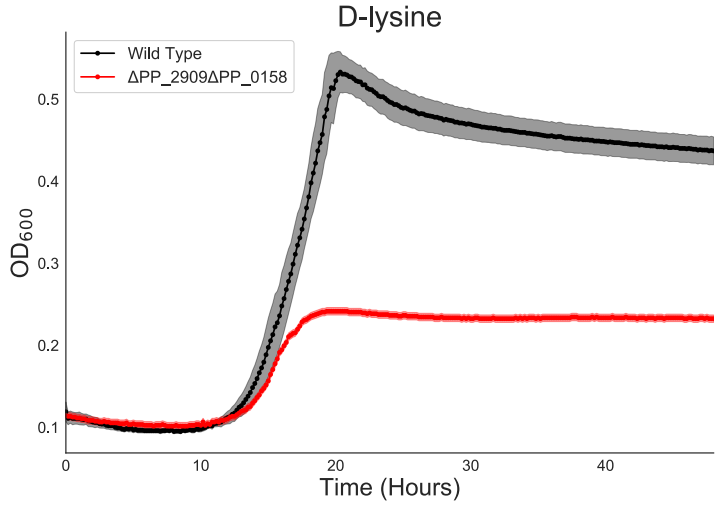
D-lysine
Wild Type
ΔPP_2909ΔPP_0158
OD600
0.1
0.2
0.3
0.4
0.5
0
10
20
30
40
Time (Hours)

B

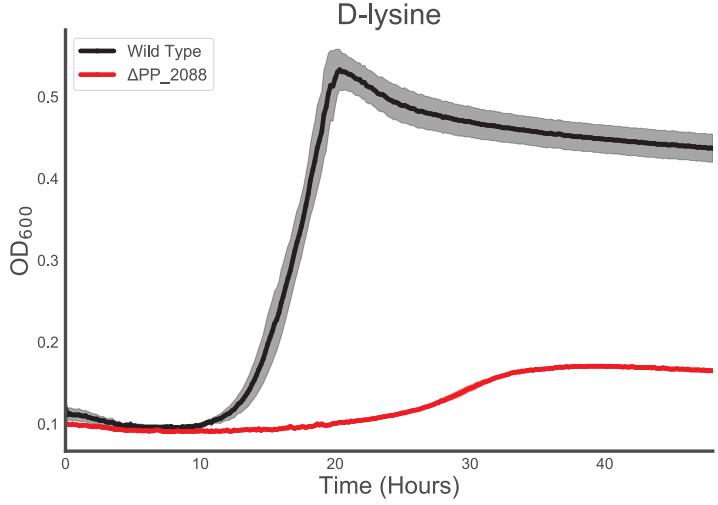
D-lysine
Wild Type
ΔPP_2088
OD600
0.1
0.2
0.3
0.4
0.5
0
10
20
30
40
Time (Hours)